Geology of the Acropolis prospect, South Australia, constrained by high-precision CA-TIMS ages

J. McPhie[a]*, K. Ehrig[b], M. B. Kamenetsky[a], J. L. Crowley[c] and V. S. Kamenetsky[a]

[a] School of Natural Sciences and CODES, University of Tasmania, Hobart, TAS, Australia; [b] BHP Olympic Dam, Level 2, 55 Grenfell St, Adelaide, SA 5000, Australia; [c] Isotope Geology Laboratory, Boise State University, Boise, Idaho, USA

*Corresponding author: j.mcphie@utas.edu.au

Jocelyn McPhie https://orcid.org/0000-0001-9147-8592

Kathy Ehrig https://orcid.org/0000-0002-5381-9445

Maya Kamenetsky https://orcid.org/0000-0002-0417-3975

James Crowley https://orcid.org/0000-0001-5069-0773

Vadim Kamenetsky https://orcid.org/0000-0002-2734-8790

Editorial handling: Anita Andrew

Received 23 October 2019; accepted 8 January 2020

SUPPLEMENTARY PAPERS

Australian Journal of Earth Sciences (2020) *67,* doi:10.1080/08120099.2020.1717617

Supplementary papers

LA-ICPMS U–Pb geochronology methods for apatite and zircon

Apatite and zircon were hand-picked from heavy fraction of crushed rocks and mounted in 1" rounds blocks using epoxy resin. The mounts were then polished using 1-micron diamond compound. After polishing the samples were cleaned in distil water in a sonic bath, rinsed several times and then being dried thoroughly.

Both apatite and zircon U–Pb geochronology were conducted on an Agilent 7900 quadrupole ICPMS coupled to a Coherent COMPex Pro 110 utilising an ArF excimer laser, operating at the 193 nm wavelength and a pulse width of ~20 ns. A RESO-lution/Laurin Technic S155 constant geometry ablation cell was used. Ablation of the various minerals took place in a helium atmosphere (0.35 l/min) that was immediately mixed with argon (~1 L/min). The signal was homogenised in a signal smoothing device (the 'squid') and finally sent into the torch of the ICP-MS. Small amounts of nitrogen gas (~1.5 ml/min) was added to the gas stream after the ablation cell to improve sensitivity. The ICP-MS is tuned daily for maximum sensitivity while keeping oxides below 0.2% (ThO/Th in a line on NIST612). Each analysis began with a 10–30 second analysis of the blank gas measurement followed by a further 20–30 seconds of acquisition time when the laser was switched on.

Apatite analyses with associated reference materials were ablated with a 29 □m spot size at 5 Hz and ~2 J/cm$_2$ laser fluence. The OD306 apatite (Thompson *et al.*, 2016) was used as a primary in-house geochronology reference material for calibration of Pb/U ratios and to correct for instrument drift (Huang *et al.*, 2015). Calibration of the ^{207}Pb/^{206}Pb ratio was done using analyses of the NIST610 reference glass analysed under the same conditions as the unknowns. The Durango (McDowell, McIntosh, & Farley, 2005), Kovdor (Amelin & Zaitsev, 2002), McClure Mountain (Schoene & Bowring, 2006), Otter Lake (Barfod, Krogstad, Frei, & Albarède, 2005) and OD401 (Thompson *et al.*, 2016) apatite were employed as secondary geochronology reference materials and were treated as unknowns.

Zircons were sampled on 29–32 µm spots using the laser at 5 Hz and approximately 2 J/cm$_2$ laser fluence. Detailed analytical method for U–Pb dating of zircon was outlined in Thompson, Meffre and Danyushevsky (2018). Zircon 91500 (^{207}Pb/^{206}Pb age = 1065.4 ± 0.3 Ma; Wiedenbeck *et al.*, 1995) was used as a primary reference material for all analyses, which were further verified by secondary reference zircons Temora (^{206}Pb/^{238}U age = 416.75 ± 0.24 Ma; Black *et al.*, 2003) and Plešovice (^{206}Pb/^{238}U date of 337.13 ± 0.37 Ma; Sláma *et al.*, 2008).

The data were reduced using an in-house excel-based spreadsheet, with error propagation following published recommendations (Horstwood *et al.*, 2016); i.e. random uncertainties as well as total uncertainties including systematic uncertainties). The data reduction was based on the method outlined in Halpin *et al.* (2014) and is similar to that outlined in Black *et al.* (2004) and Paton *et al.* (2010). The program Isoplot 4.11 (Ludwig, 2008) was used for Tera-Wasserburg concordia plots and age calculations.

Description of geochronology samples

Drill hole	Depth (m)	Field #	Description
ACD2	673.4	OD20	Feldspar-phyric rhyolite: Ti/Zr ~6–7. Purplish grey aphanitic groundmass; white prismatic feldspar phenocrysts (~10 modal%, 6–8 mm). Moderately altered, abundant Fe oxide veins.
ACD2	795.7	OD22	Fine breccia: Massive, poorly sorted breccia composed of angular pink clasts (2–4 cm) in fine grey sandstone matrix; bed <1 m thick between rhyolite units.
ACD2	907.2	OD23	Feldspar-phyric rhyolite: Ti/Zr ~7–8. Massive, pink aphanitic groundmass; green prismatic feldspar phenocrysts (~7 modal%, 6–10 mm). Moderately altered.
ACD7	599	OD1199-RX8078	Granite: Mottled pink-green-grey equigranular, medium grained, massive granite composed of pink or green-grey feldspar and subordinate quartz. Moderately altered.
ACD19	845	OD1178	Felsic dyke/sill: Ti/Zr ~5, rhyolite. Mottled pink-green aphanitic groundmass; cream-pale green, prismatic feldspar phenocrysts (~5 modal%, 5–10 mm). Weakly altered. Sharp contacts at 841 and 850 m.
ACD19	936.3	OD1182	Laminated clastic facies: Pink versus grey, planar laminae composed of mudstone and well sorted quartzo-feldspathic sandstone; strongly magnetic. Narrow (mm–cm) Fe oxide–sulfide veins.
ACD20	816.4	OD419	Ignimbrite: Ti/Zr 7–10. Dark green-grey, wispy fiamme (1–6 cm long) and sparse lithic fragments (1–2 cm) in pink matrix; aphyric(?) or crystal-poor (<1 modal%, feldspar, <0.5 mm). Strongly altered.
ACD20	827.5	OD420	Megacrystic granite: Pink feldspar crystals (1–5 cm) dispersed in grey, finer (1–4 mm), equigranular, quartz–feldspar–ferromagnesian assemblage. Ferromagnesian phase completely altered to green chlorite. Overall, weakly altered.
ACD21	535	OD1196	Feldspar-phyric dacite: Ti/Zr ~20. Massive, pink-red-brown aphanitic groundmass; cream or dark green prismatic feldspar phenocrysts (~7 modal%, 2–8 mm). Quartz-filled amygdales (2–5 mm); locally monomictic breccia. Weakly altered, narrow (mm) Fe oxide veins.
ACD21	726.3	OD1197	Felsic dyke/sill: Ti/Zr 7–10, rhyolite. Red aphanitic ground mass; pink-cream feldspar (1–8 mm) and quartz (1–6 mm) phenocrysts (10–15 modal% total). Weakly altered. Sharp contacts at 724.6 m and 742 m.

Figures S1–S16. Stratigraphic and Ti/Zr logs for drill holes.

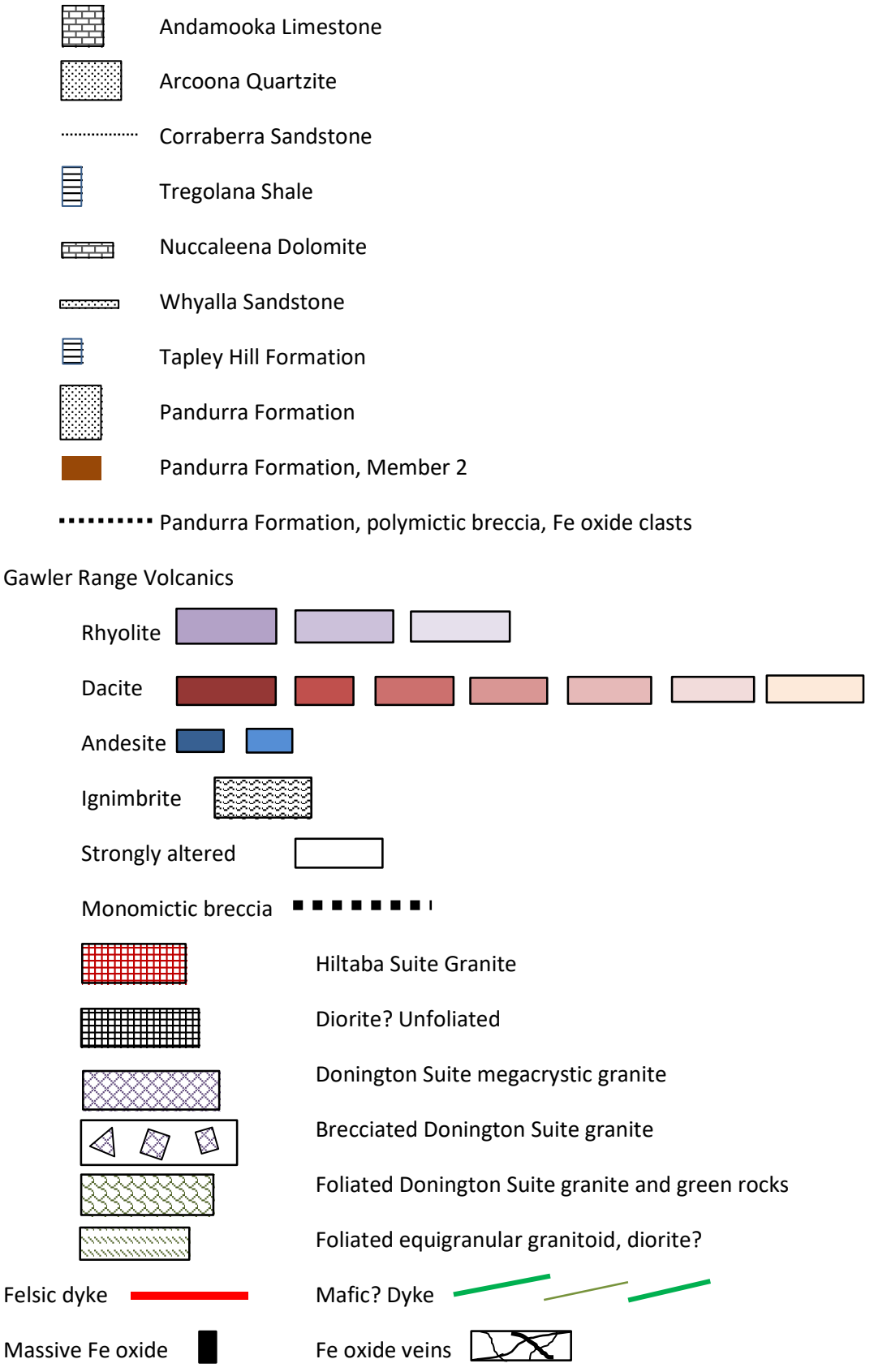

Figure S1a. Legend for lithologies shown on Acropolis drill hole logs.

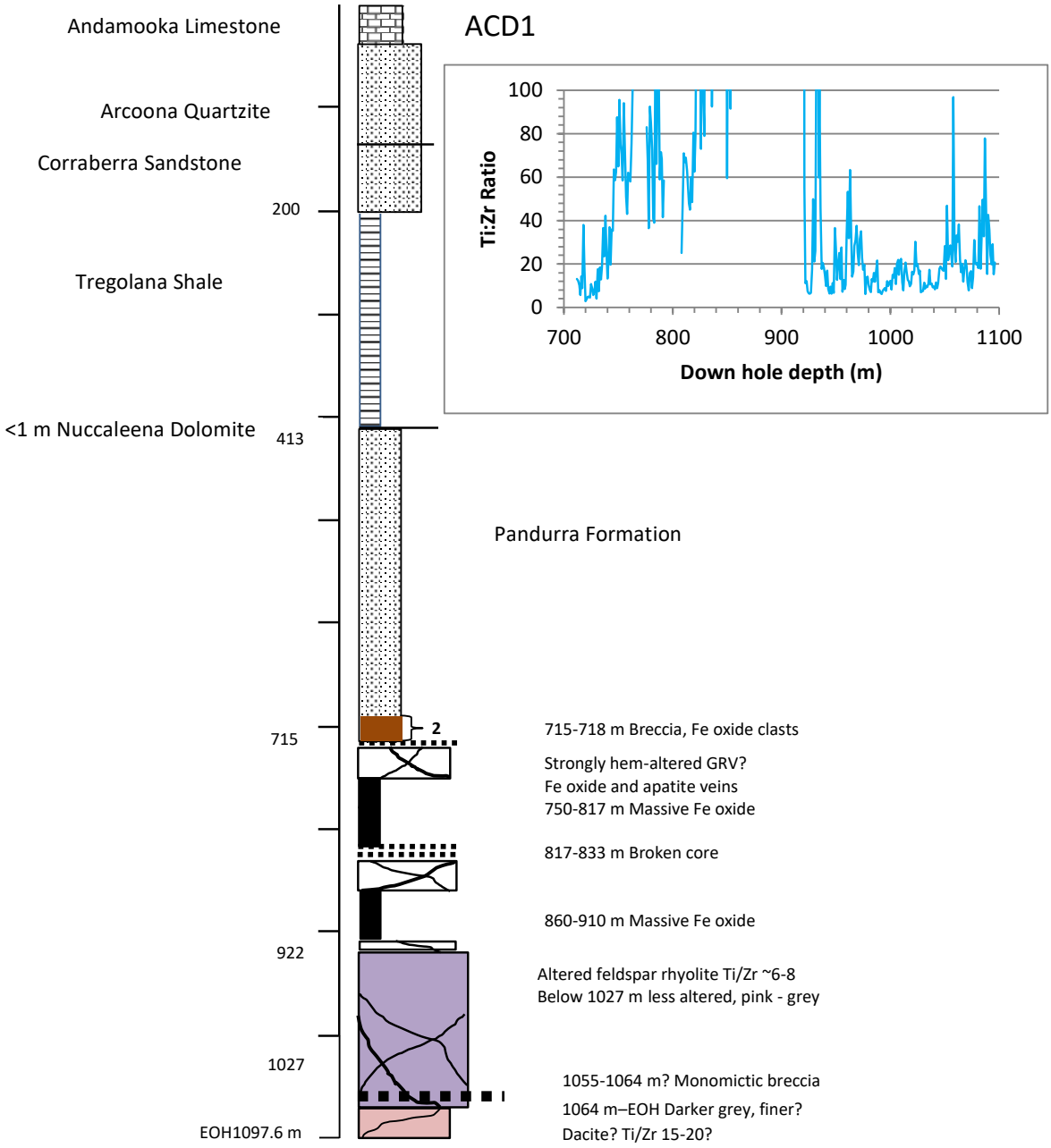

Figure S1b. ACD1. The GRV (718-1097.6 m) section is ~380 m thick. The top part (~204 m) is very strongly altered and includes thick intervals of massive Fe oxide (drill hole was probably drilled along steeply dipping Fe oxide veins). Below ~922 m, the alteration intensity and Fe oxide abundance diminish, and it could be that a fault separates the upper strongly altered interval from the lower less altered interval. The less altered GRV comprises feldspar-phyric rhyolite(?) (922-1064 m) overlying fine dark-grey dacite(?)(1064 m to EOH). Bracket and "2" are Member 2 of the Pandurra Formation according to Cowley (1993). Inset gives the downhole Ti:Zr data from 1-m interval assays.

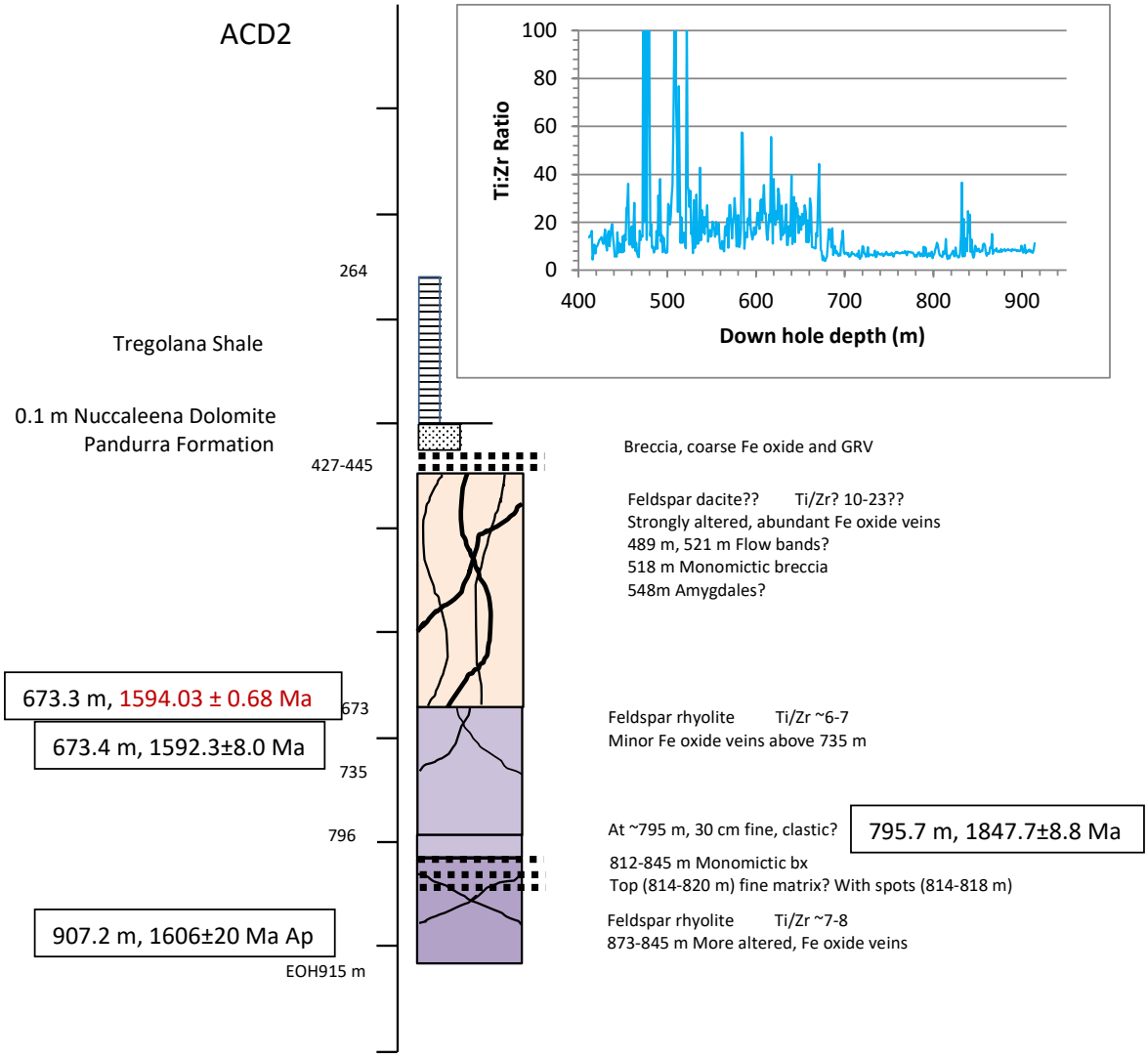

Figure S2. ACD2. The GRV (445-915 m) section is ~470 m thick. The top part (~228 m) is more strongly altered than the lower part and includes abundant Fe oxide veins. The Ti/Zr of the strongly altered interval shows the effects of alteration but appears to be higher (mostly >10) than the Ti/Zr of the lower part (<8). Breaks between successive feldspar-phyric rhyolite units occur at ~795 m and ~812-845 m, the latter including distinctive spotty texture. Four ages have been determined - three using LA-ICPMS (two on zircon, one on apatite (Ap)) and one using CA-TIMS (red font) (Table 1). Inset gives the downhole Ti/Zr data from 1-m interval assays.

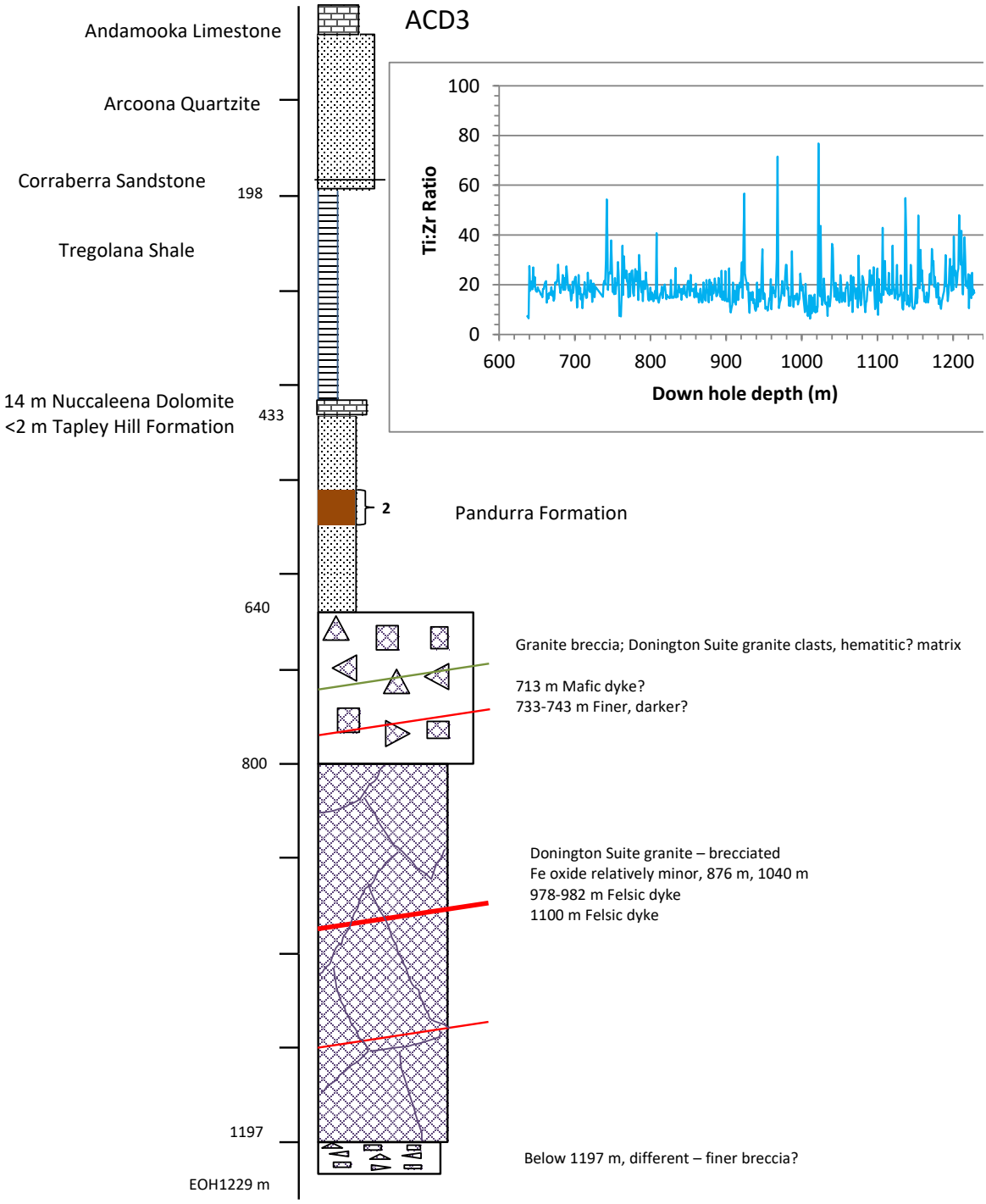

Figure S3. ACD3. This drill hole is east of an inferred fault that separates GRV to the west from pre-GRV basement units to the east, so there is no GRV preserved. The main lithology is Donington Suite foliated megacrystic granite. The granite is intensely (above ~800 m) to moderately brecciated so the drill hole could have been drilled along or close to a fault. At least one mafic and three felsic dykes appear to cut the brecciated Donington Granite; the dykes could therefore post-date the brecciation/fault. The breccia below ~1197 m is finer. Bracket and "2" are Member 2 of the Pandurra Formation according to Cowley (1993). Inset gives the downhole Ti:Zr data from 1-m interval assays.

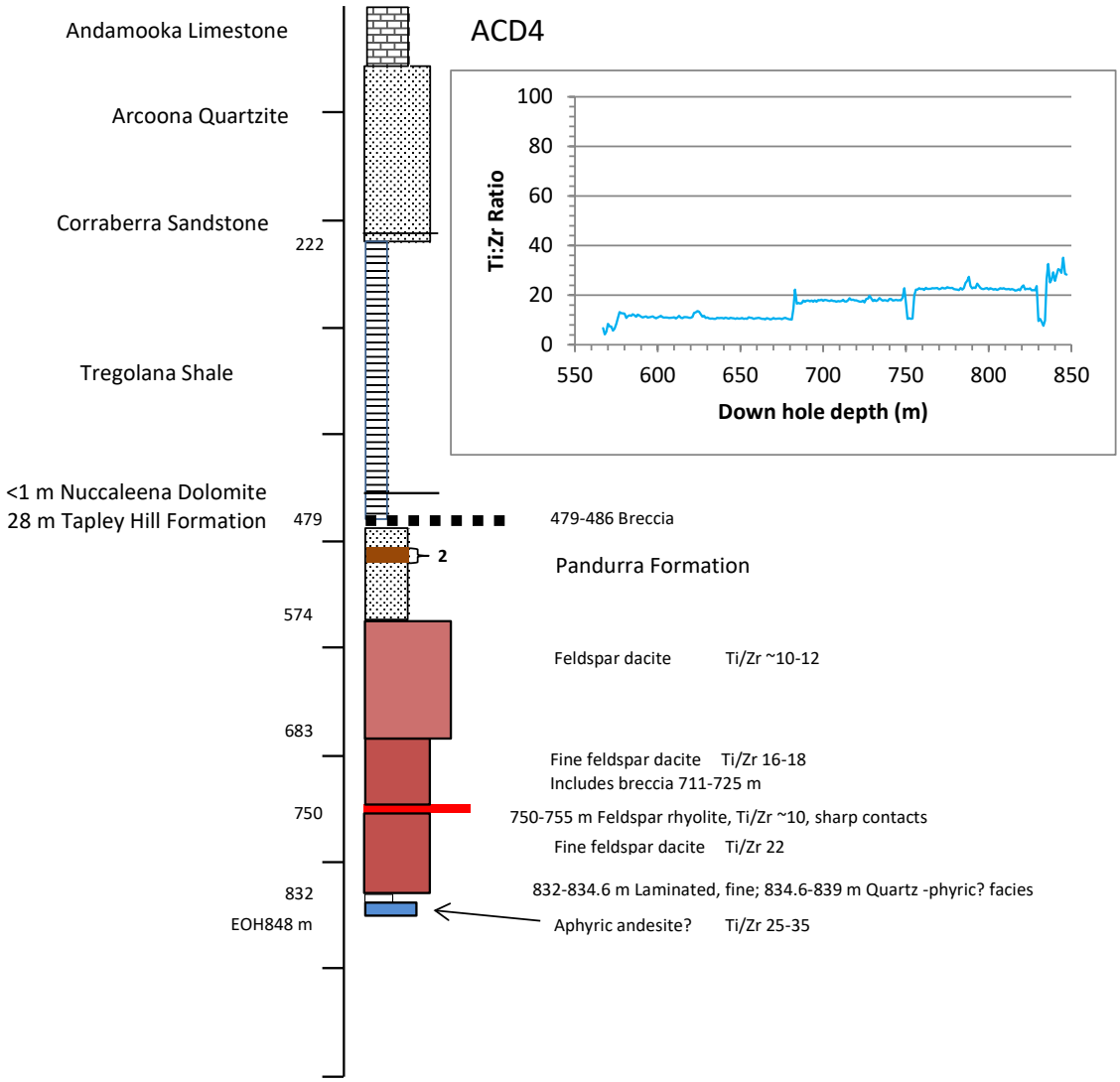

Figure S4. ACD4. The GRV section (574-848 m) is ~274 m thick and mostly comprises weakly altered dacitic units. The downhole Ti:Zr profile reflects the volcanic units very well. The narrow interval of feldspar-phyric rhyolite (750-755 m) is probably a dyke or sill. The drill hole intersected laminated clastic facies and a quartz-phyric(?) unit near the base and ended in andesite(?). This drill hole does not have the GRV ignimbrite found in ACD19 which is <2 km to the south-southeast, but the lowermost fine feldspar-phyric dacite (Ti/Zr ~22) could match the uppermost fine feldspar-phyric dacite in ACD19 (Ti:Zr 20-22). Bracket and "2" are Member 2 of the Pandurra Formation according to Cowley (1993). Inset gives the downhole Ti:Zr data from 1-m interval assays.

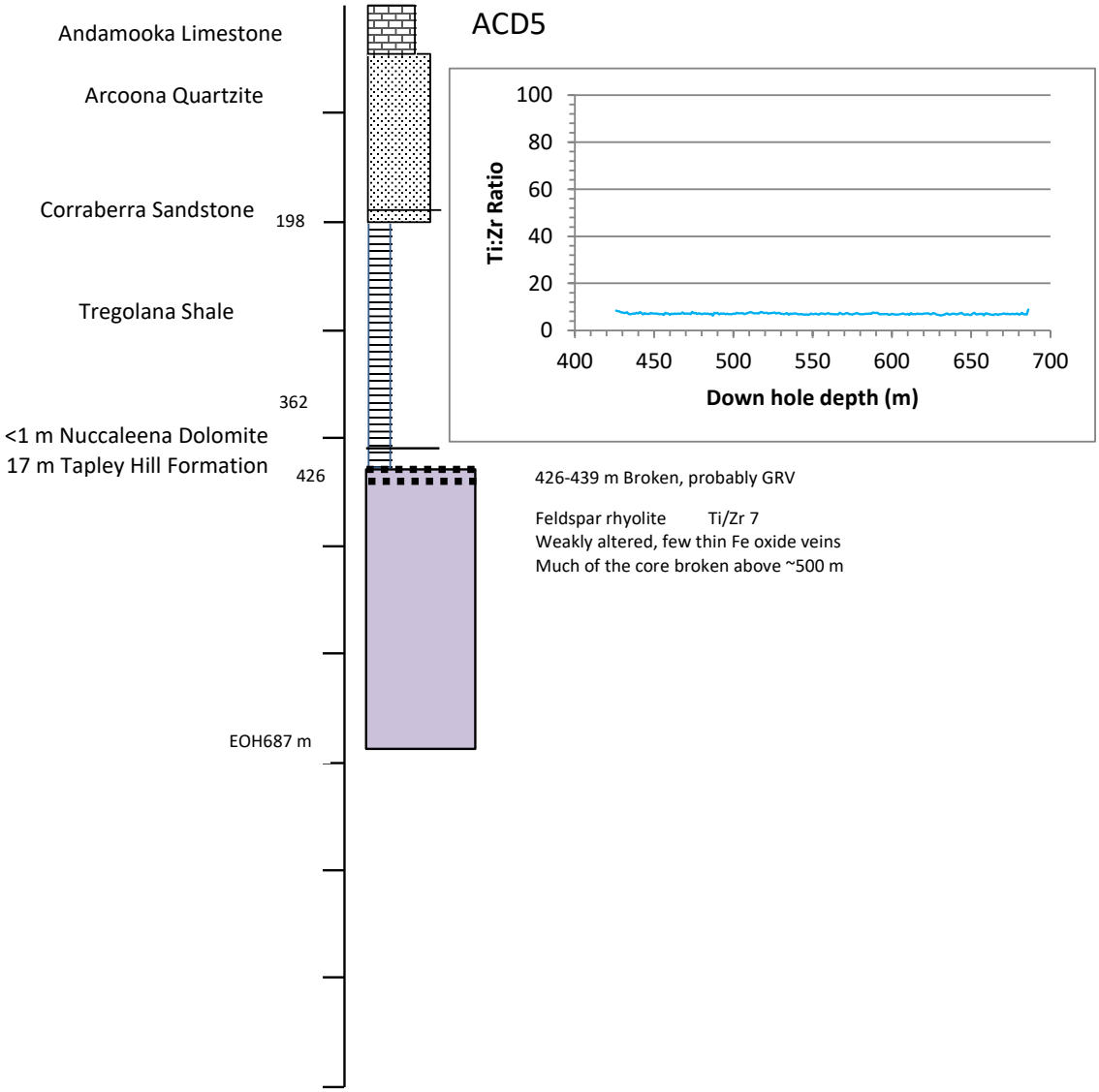

Figure S5. ACD5. The GRV section (426-687 m) is ~261 m thick and comprises weakly altered feldspar-phyric rhyolite. The drill core is noticeably broken and somewhat more altered above ~500 m. Texturally similar feldspar-phyric rhyolite that occurs in holes in the southwestern part of the area (e.g. ACD1, ACD9, ACD10) is much more strongly altered and has a much higher abundance of Fe oxide veins. Notable in this hole is the absence of the Pandurra Formation, suggesting that this location was a GRV-age topographic high when the Pandurra Formation was being deposited. Alternatively, this location was up-faulted to a topographically high position after deposition of the Pandurra Formation and the Pandurra Formation was then completely eroded. Inset gives the downhole Ti:Zr data from 1-m interval assays.

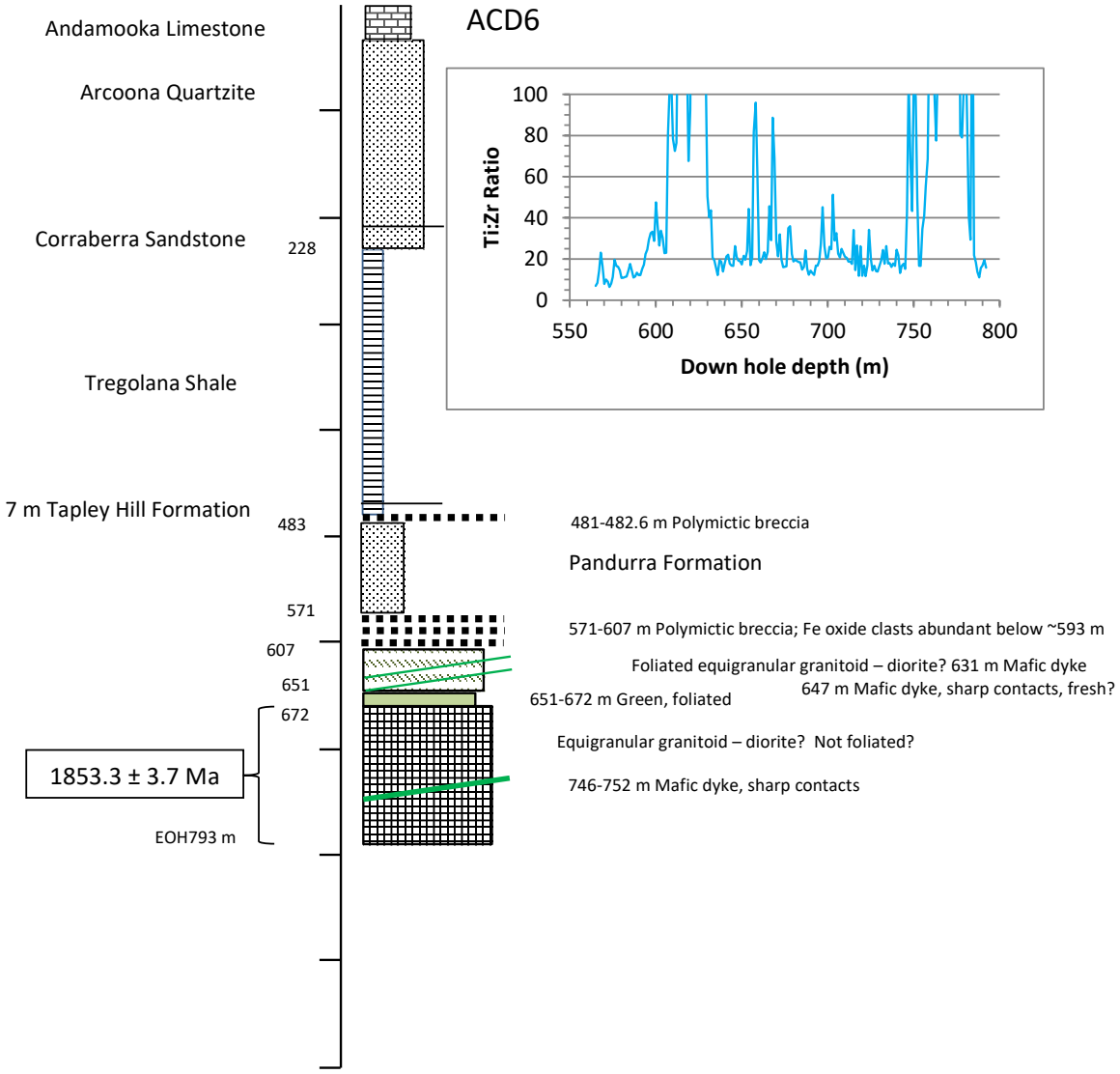

Figure S6. ACD6. This drill hole is east of an inferred fault that separates GRV to the west from pre-GRV basement units to the east, so there is no GRV section preserved. The main lithology is equigranular diorite(?) for which Jagodzinski (2005) reported a SHRIMP U-Pb in zircon age of 1853.3 ± 3.7 Ma. The diorite(?) and another finer? green lithology are foliated above 672 m. At least three mafic dykes appear to cut the diorite(?). Inset gives the downhole Ti:Zr data from 1-m interval assays.

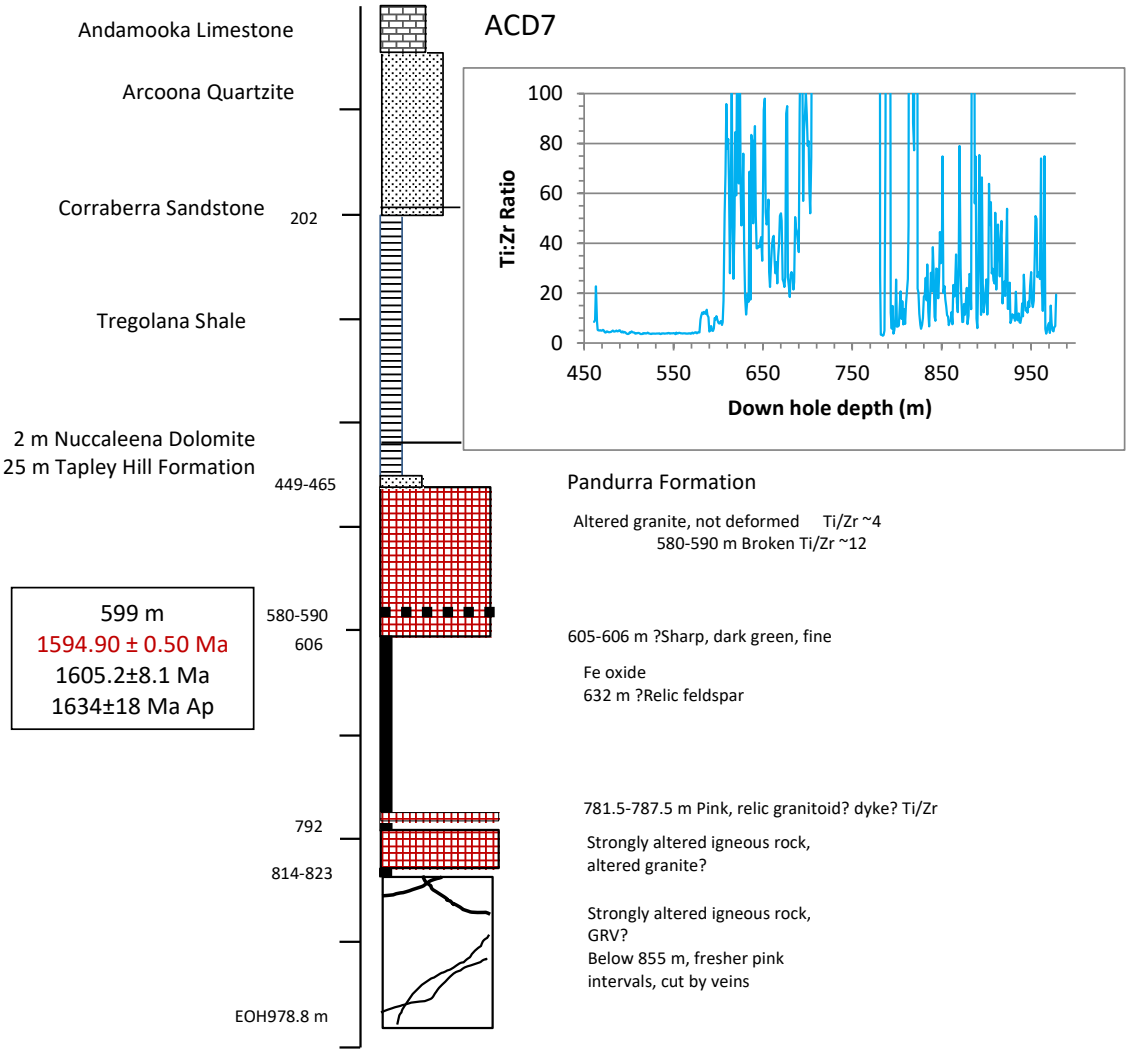

Figure S7. ACD7. The pre-Pandurra Formation part of the section (465-978.8 m) is strongly altered. The top ~360 m consists of altered, equigranular, non-foliated granite that includes Fe oxide veins and thick intervals of massive Fe oxide (drill hole was probably drilled along steeply dipping Fe oxide veins). Three ages determined on this granite (two using LA-ICPMS, one on zircon, one on apatite (Ap) and one using CA-TIMS (red font)) indicate that it belongs to the Hiltaba Suite (Table 1). Below ~823 m, the lithology could be more of the same altered granite or altered GRV (as logged by R Uphill). If the latter is correct, then the unit could be dacite or rhyolite (Ti:Zr has been strongly affected by the Fe oxide veins). The Pandurra Formation is very thin compared with drill holes nearby to the southwest (121 m and 233 m) and south (>510 m). Inset gives the downhole Ti:Zr data from 1-m interval assays.

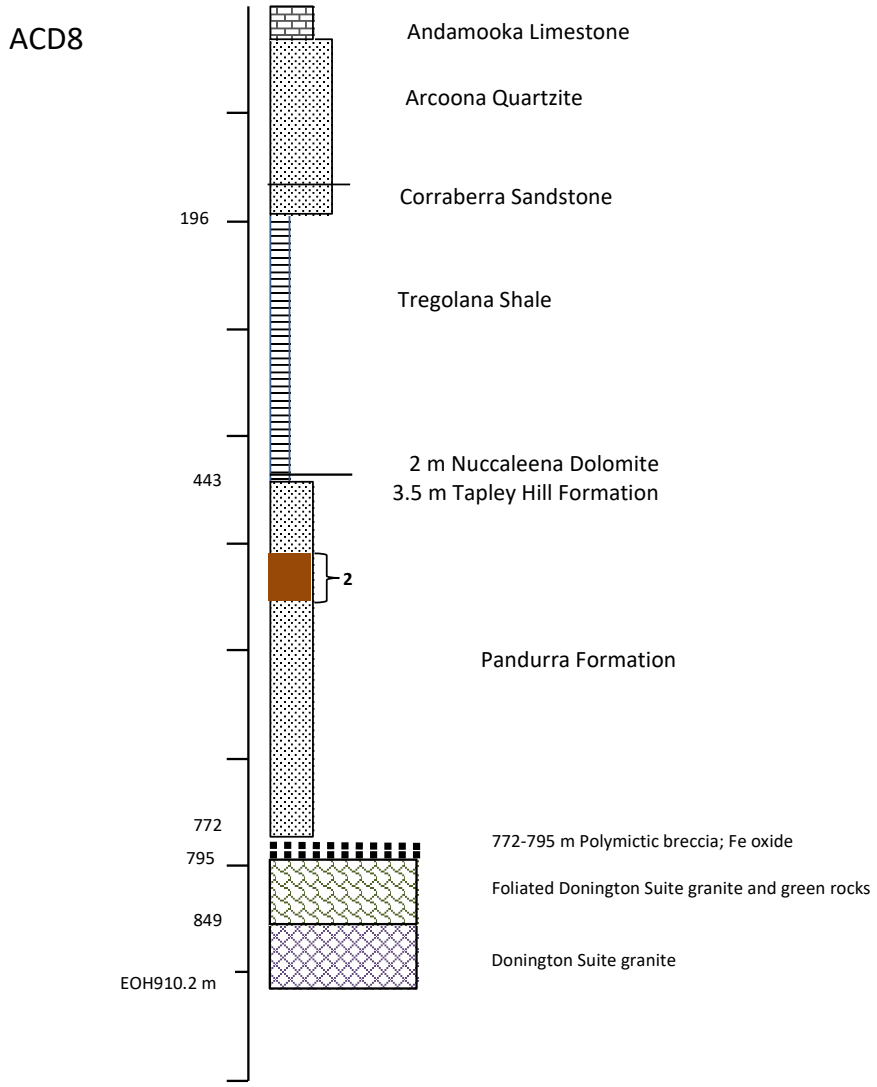

Figure S8. ACD8. The main lithology below the Pandurra Formation is foliated megacrystic granite (795-910.2 m) assumed to be the Donington Suite. The granite is more strongly foliated and altered above ~849 m but the abundance of Fe oxide veins is low throughout. Bracket and "2" are Member 2 of the Pandurra Formation according to Cowley (1993).

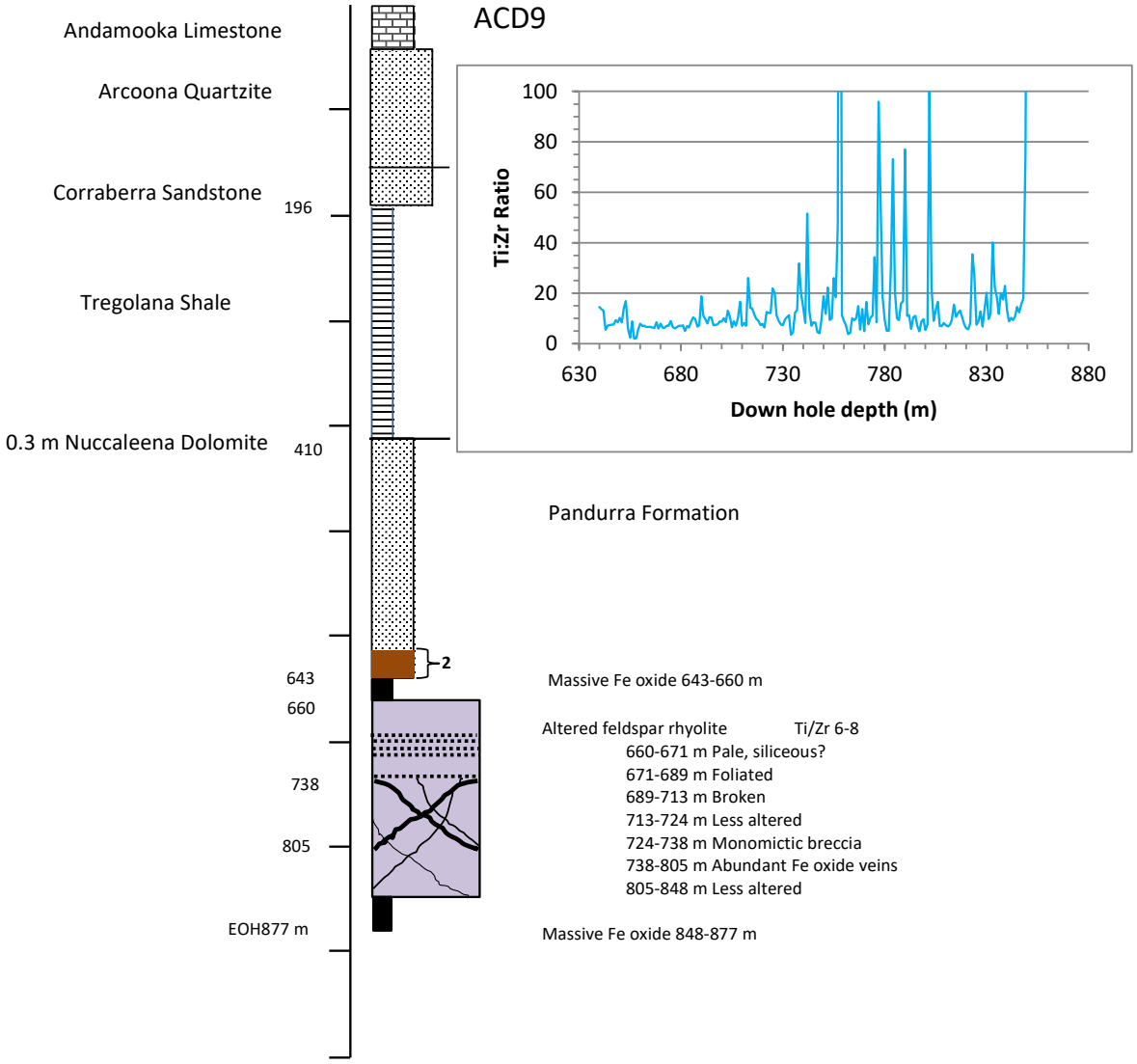

Figure S9. ACD9. The GRV (643-877 m) section is ~234 m thick and strongly altered, and includes thick intervals of massive Fe oxide (drill hole was probably partly drilled along steeply dipping Fe oxide veins). The altered feldspar-phyric rhyolite is similar to altered feldspar-phyric rhyolite in ACD1 and ACD10, and at the base of ACD2. Bracket and "2" are Member 2 of the Pandurra Formation according to Cowley (1993). Inset gives the downhole Ti:Zr data from 1-m interval assays.

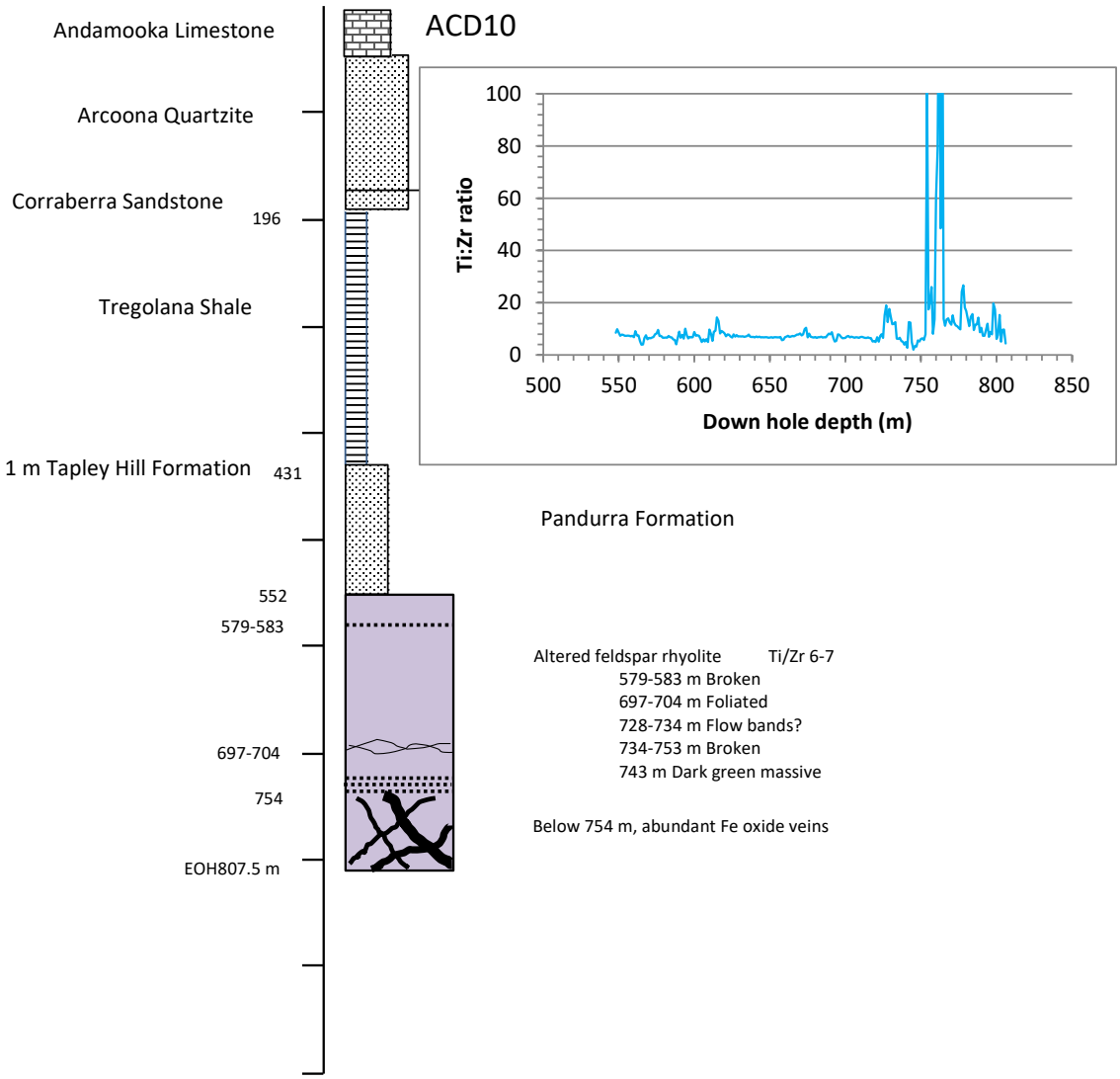

Figure S10. ACD10. The GRV (552-807.5 m) section is ~256 m thick and strongly altered; Fe oxide veins are abundant below ~754 m. The altered feldspar-phyric rhyolite is similar to altered feldspar-phyric rhyolite in ACD1 (Fig. S1) and ACD9 (Fig. S9), and at the base of ACD2 (Fig. S2). Inset gives the downhole Ti:Zr data from 1-m interval assays.

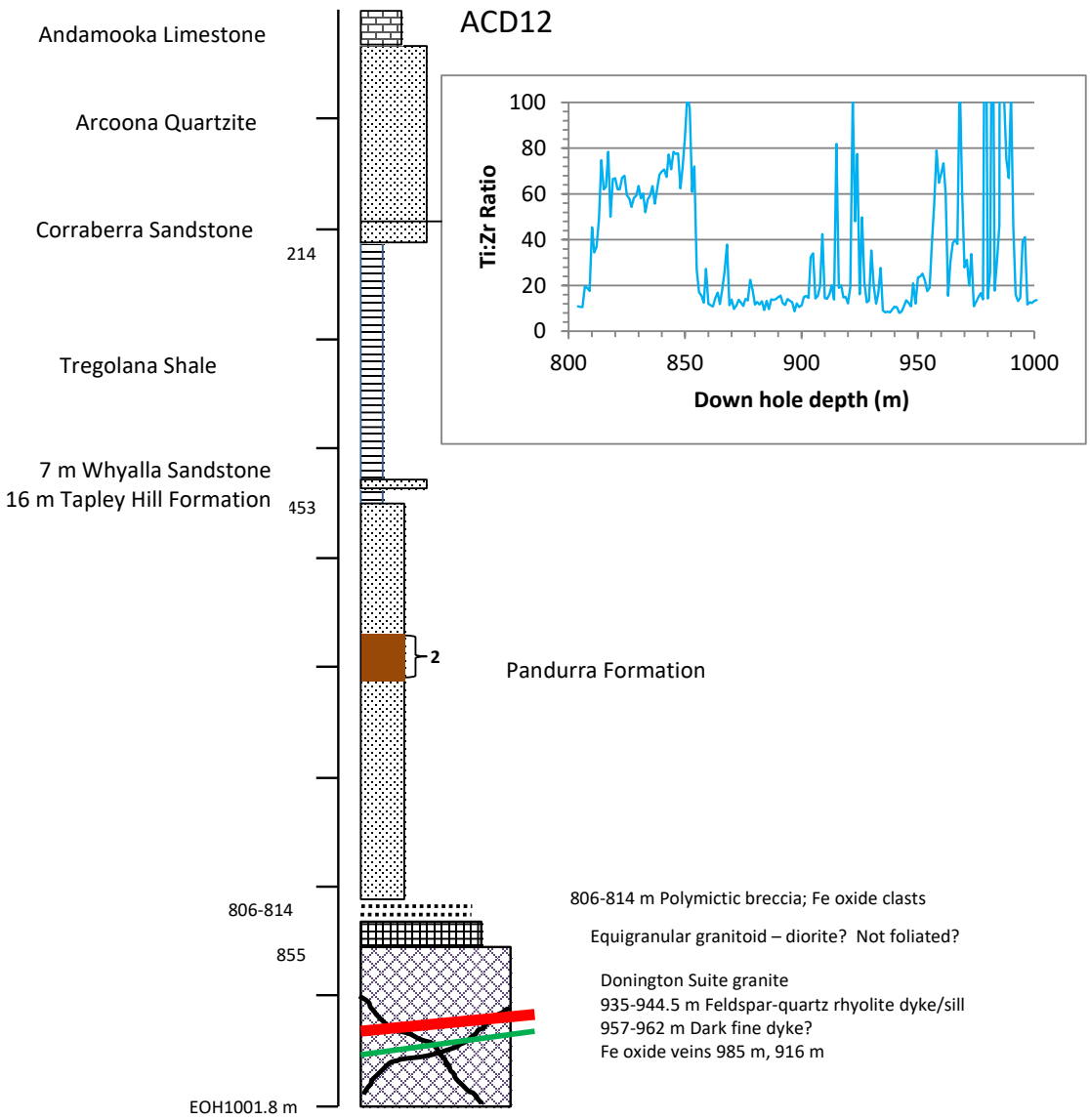

Figure S11. ACD12. This drill hole is east of an inferred fault that separates GRV to the west from pre-GRV basement units to the east, so there is no GRV preserved. Equigranular diorite(?) assumed to belong to pre-GRV basement occurs above foliated megacrystic granite assumed to belong to the Donington Suite. The diorite(?) is similar to diorite(?) in ACD6 ~4.5 km to the north (Fig. S6). A red feldspar-quartz-phyric rhyolitic dyke/sill (undeformed, no Fe oxide veins, weakly altered) intrudes the megacrystic granite; this dyke/sill is similar to felsic dykes/sills that intrude the Donington Suite in ACD3 (Fig. S3) and intrude the GRV in ACD19 (Fig. S14) and ACD21 (Fig. S16). Bracket and "2" are Member 2 of the Pandurra Formation according to Cowley (1993). Inset gives the downhole Ti:Zr data from 1-m interval assays.

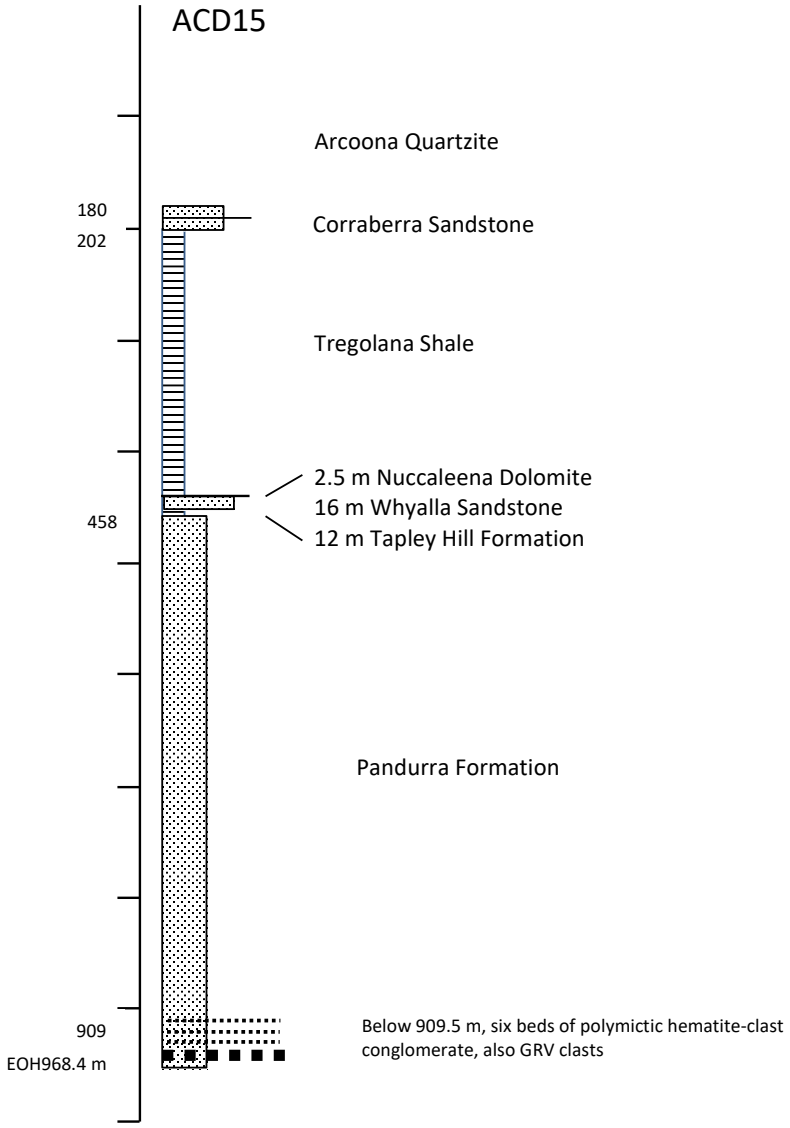

Figure S12. ACD15. No GRV was intersected in this hole. The beds of polymictic hematite-clast conglomerate that occur at the base of the hole are typical of facies found at the base of the Pandurra Formation where it overlies GRV or older basement lithologies in other drill holes, so the base of this drill hole is probably very close to the base of the Pandurra Formation. Volcanic clasts occur in the conglomerate so it is likely that the Pandurra Formation overlies GRV (rather than older basement). The Pandurra Formation is very thick (>510 m) – thicker than in any other Acropolis holes and much thicker than the nearby holes.

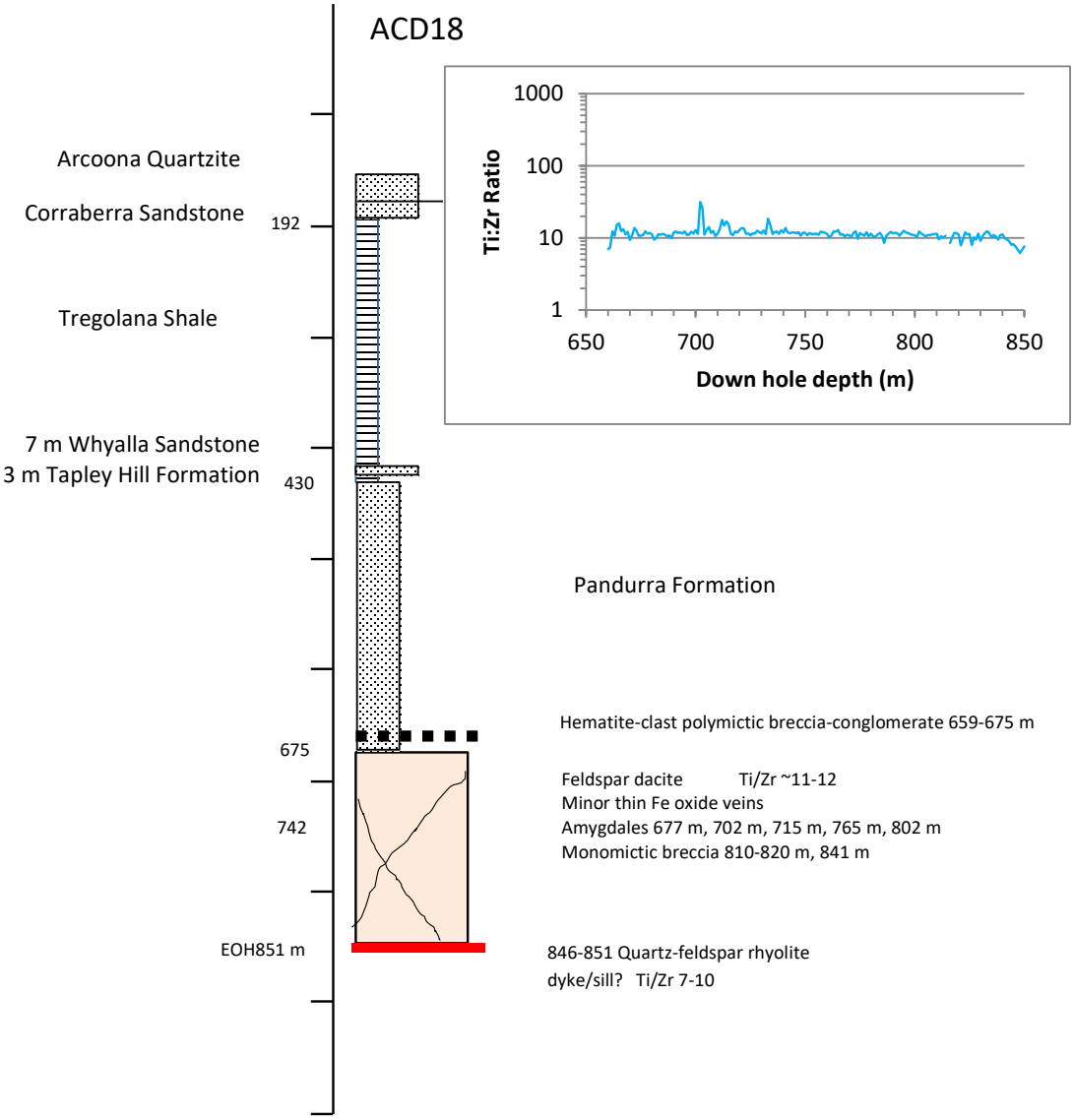

Figure S13. ACD18. The GRV (675-851 m) section is ~175 m thick, most of which appears to comprise moderately altered feldspar-phyric dacite that is cut by numerous thin Fe oxide veins. The lowest ~5 m at the base of the drill hole could be a quartz-feldspar-phyric rhyolite dyke/sill, or else the top of another GRV unit; the top contact is sharp and marked by broken core (fault?). Inset gives the downhole Ti:Zr data from 1-m interval assays.

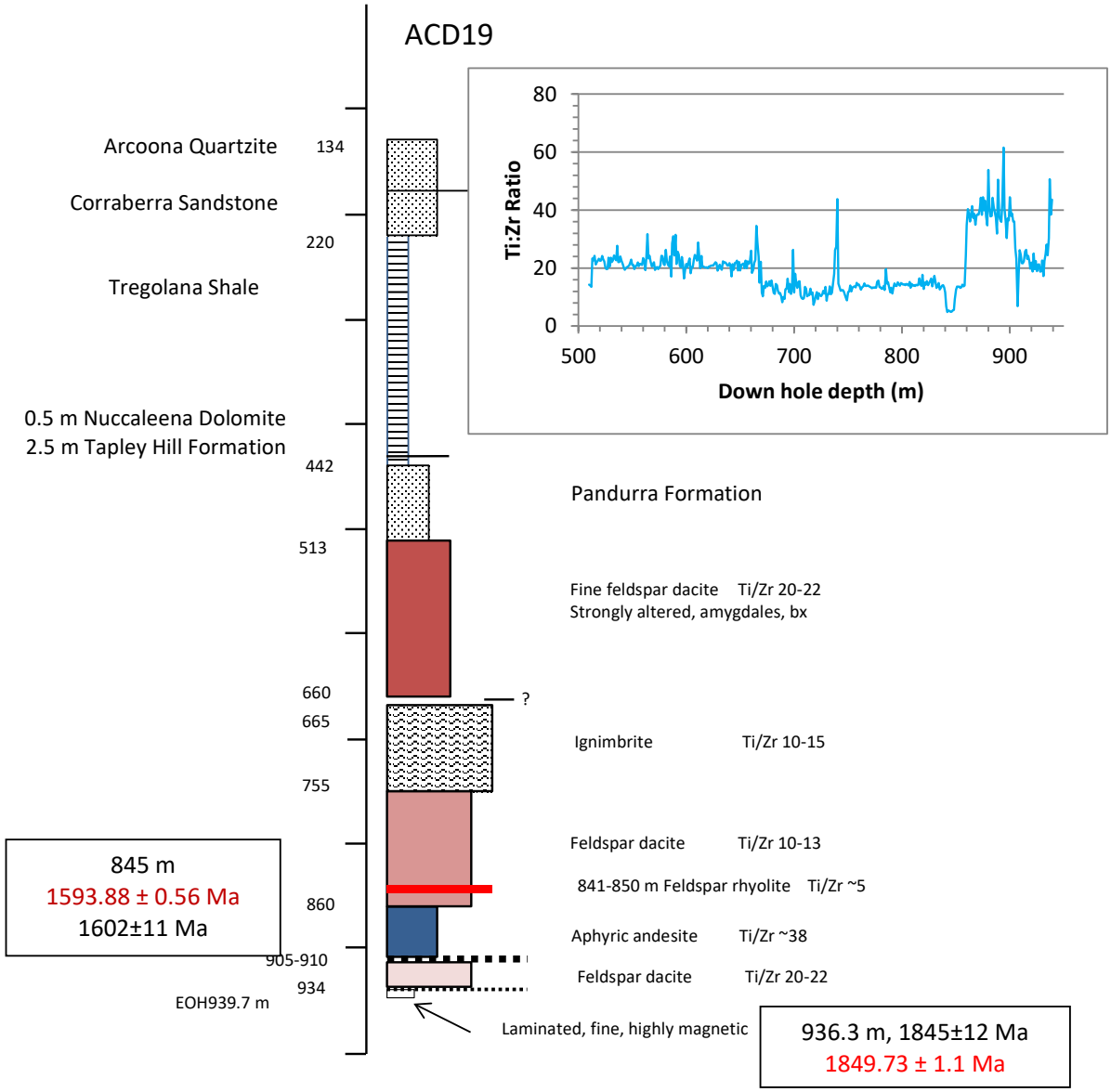

Figure S14. ACD19. The GRV (513-939.7 m) section is ~427 m thick and comprises variably altered dacite units interbedded with strongly altered ignimbrite and aphyric andesite. The volcanic units correspond closely with the Ti:Zr profile; Fe oxide veins are minor and thin. The narrow interval of feldspar-phyric rhyolite (841-850 m) is probably a dyke or sill, consistent with its age (red font, CA-TIMS, black font, LA-ICPMS) being slightly younger than that of the GRV. The drill hole ended in strongly magnetic, laminated clastic facies, the LA-ICPMS zircon age of which indicates a Donington Suite provenance. The uppermost fine feldspar-phyric dacite (Ti:Zr 20-22) could match the lowermost fine feldspar-phyric dacite (Ti:Zr ~22) in ACD4 (Fig. S4) which is <2 km to the north-northwest. Inset gives the downhole Ti:Zr data from 1-m interval assays.

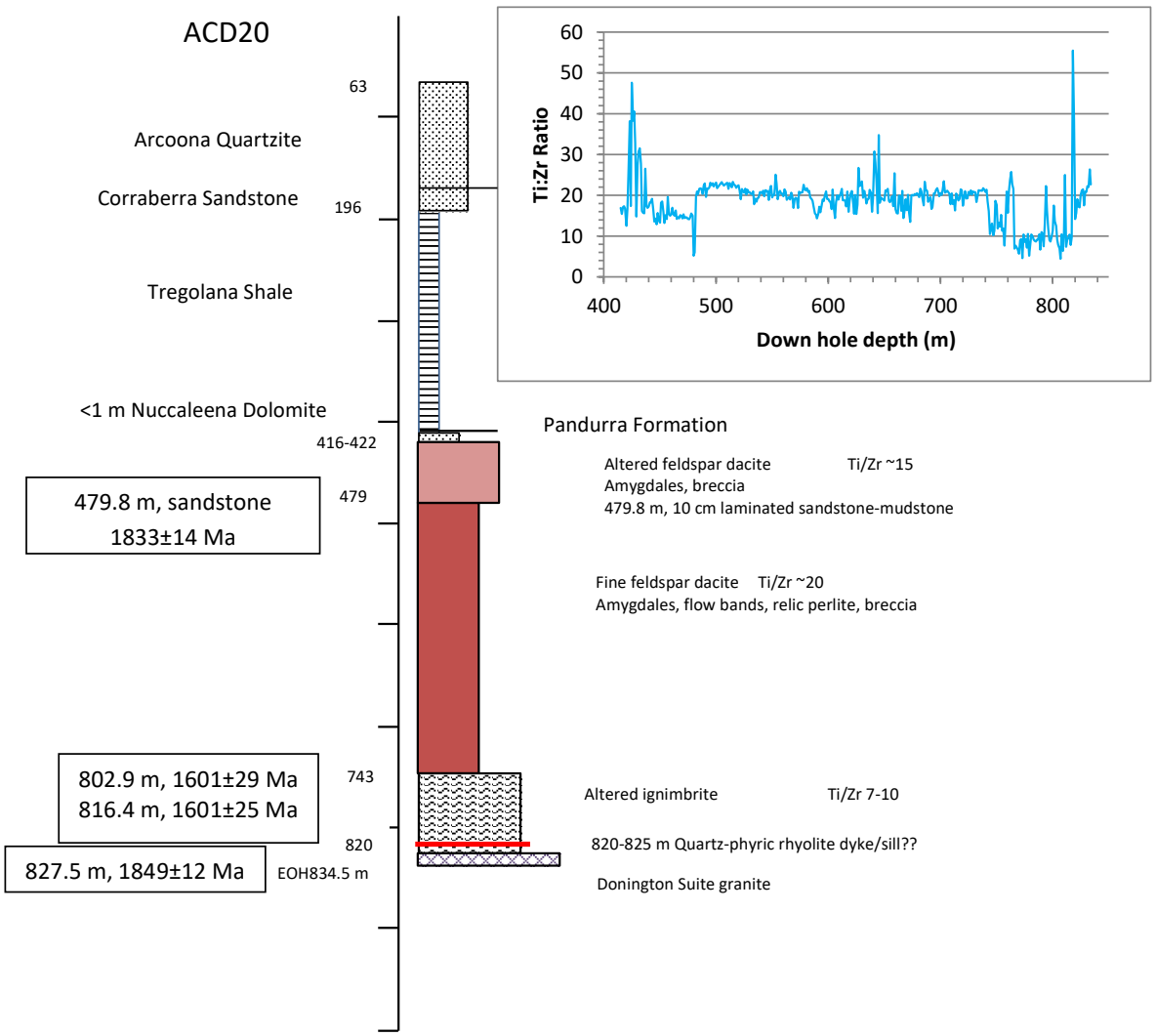

Figure S15. ACD20. The GRV (422-820 m) section is ~398 m thick and comprises weakly altered dacite units above strongly altered ignimbrite. The ignimbrite overlies altered megacrystic granite (Donington Suite) but the contact is complicated by a quartz-phyric rhyolite dyke/sill (~820-825 m). The fine feldspar-phyric dacite (Ti/Zr ~20) and altered ignimbrite in this drill hole can be correlated with similar units in ACD19 (Fig. S14) which occurs ~3 km to the north-northwest. However, none of the pre-Pandurra Formation section in this drill hole correlates with drill holes nearby to the west (ACD7, ~2 km west-northwest; Fig. S7) or to the east (ACD6, ~1.5 km east; Fig. S6). Although imprecise, the LA-ICPMS zircon ages confirm the affinity of the GRV units and the Donington Suite, and reveal the Donington Suite provenance of sandstone interbedded in the GRV. Inset gives the downhole Ti:Zr data from 1-m interval assays.

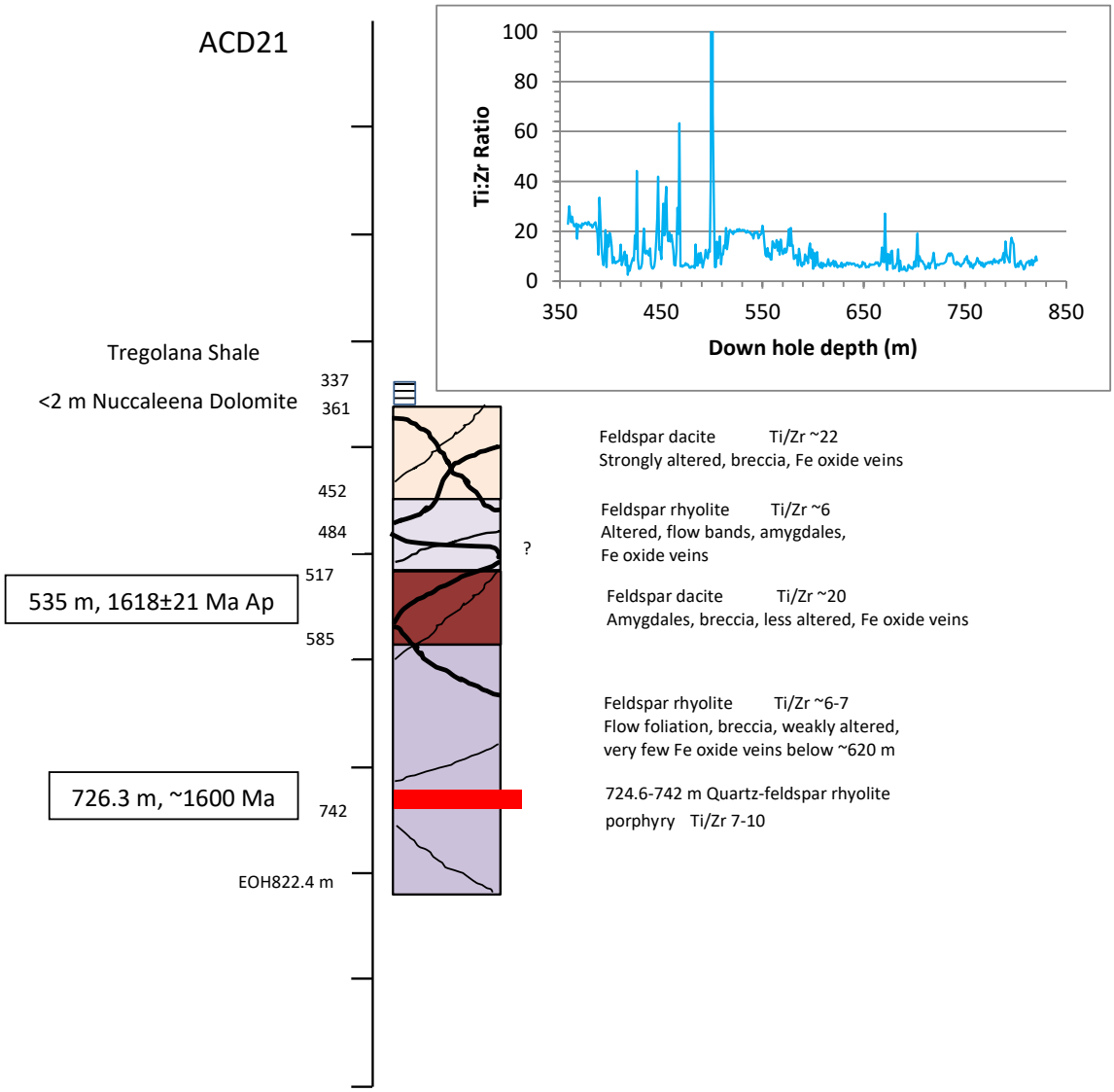

Figure S16. ACD21. The GRV (361-822.4 m) section is more than 461 m thick and comprises feldspar-phyric dacite and rhyolite units. The intensity of alteration is higher above ~517 m and the abundance and size of Fe oxide veins is noticeably lower below ~620 m. The GRV section in this drill hole is broadly similar to the GRV in ACD2 ~1 km to the northwest (Fig. S2) but cannot be matched with the single GRV unit in ACD18 ~1 km to the east (Fig. S13). A red quartz-feldspar-phyric rhyolitic dyke/sill (724.6-742 m; undeformed, no Fe oxide veins, weakly altered) intrudes the lower feldspar-phyric rhyolite. Similar felsic dykes/sills intrude the Donington Suite in ACD3 (Fig. S3) and ACD12 (Fig. S11) about 2 km to the east. Two imprecise LA-ICPMS ages were obtained for the GRV section (one on zircon, one on apatite). The Pandurra Formation is missing. Inset gives the downhole Ti:Zr data from 1-m interval assays.

Figures S17 and S18. LA-ICPMS isochrons for Acropolis samples.

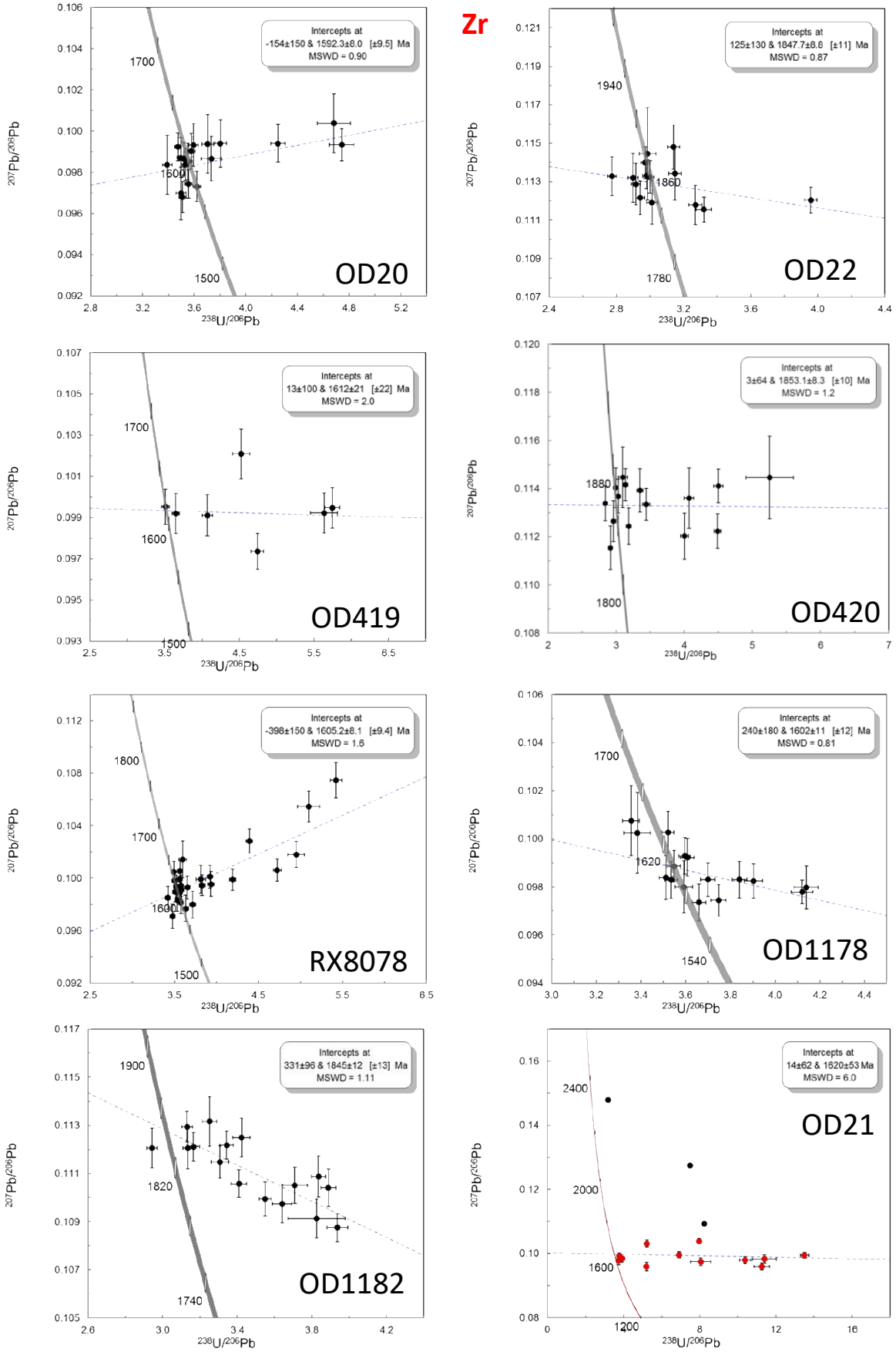

Figure S17. Zircon LA-ICPMS isochrons for Acropolis samples.

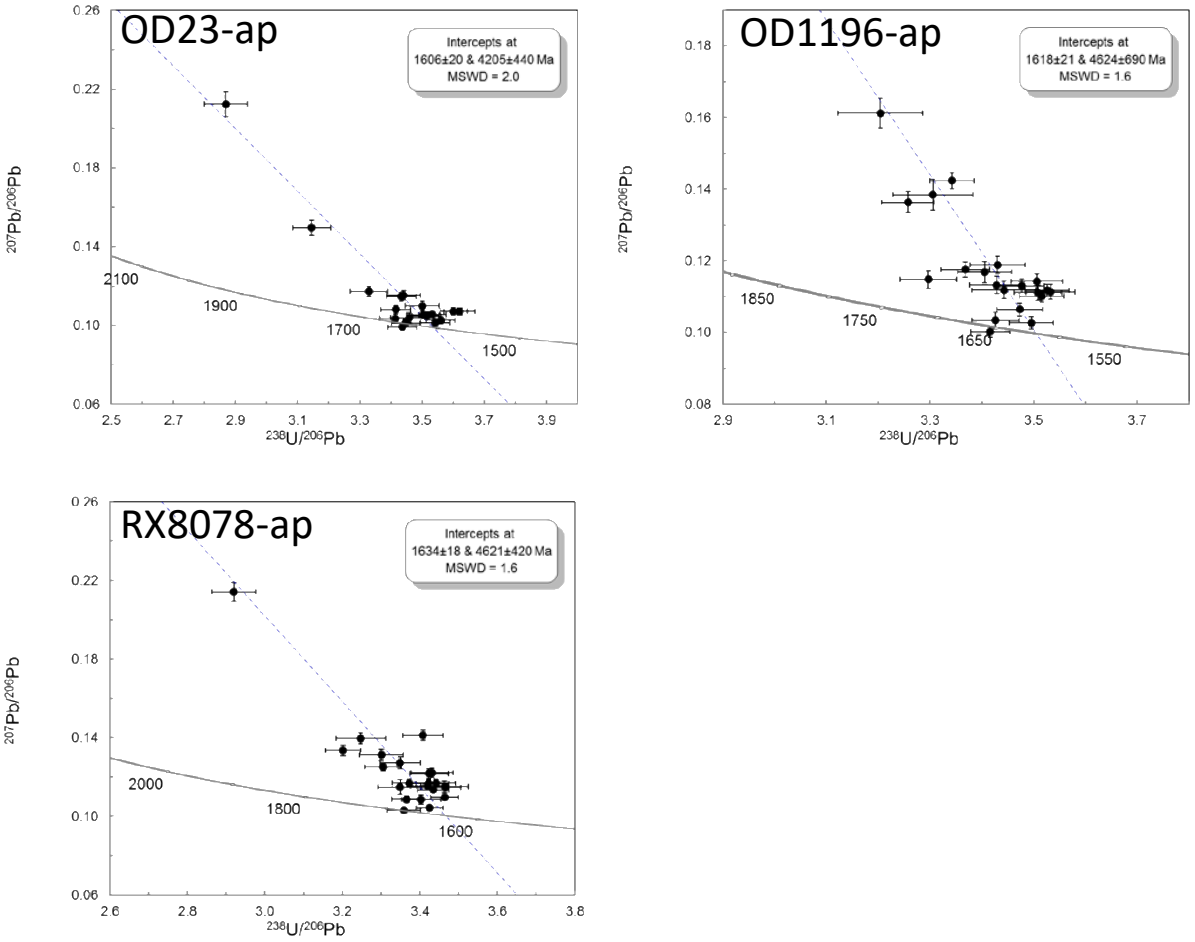

Figure S18. Apatite LA-ICPMS isochrons for Acropolis samples.

Figures S19–S23. Cathodoluminescence images of zircons.

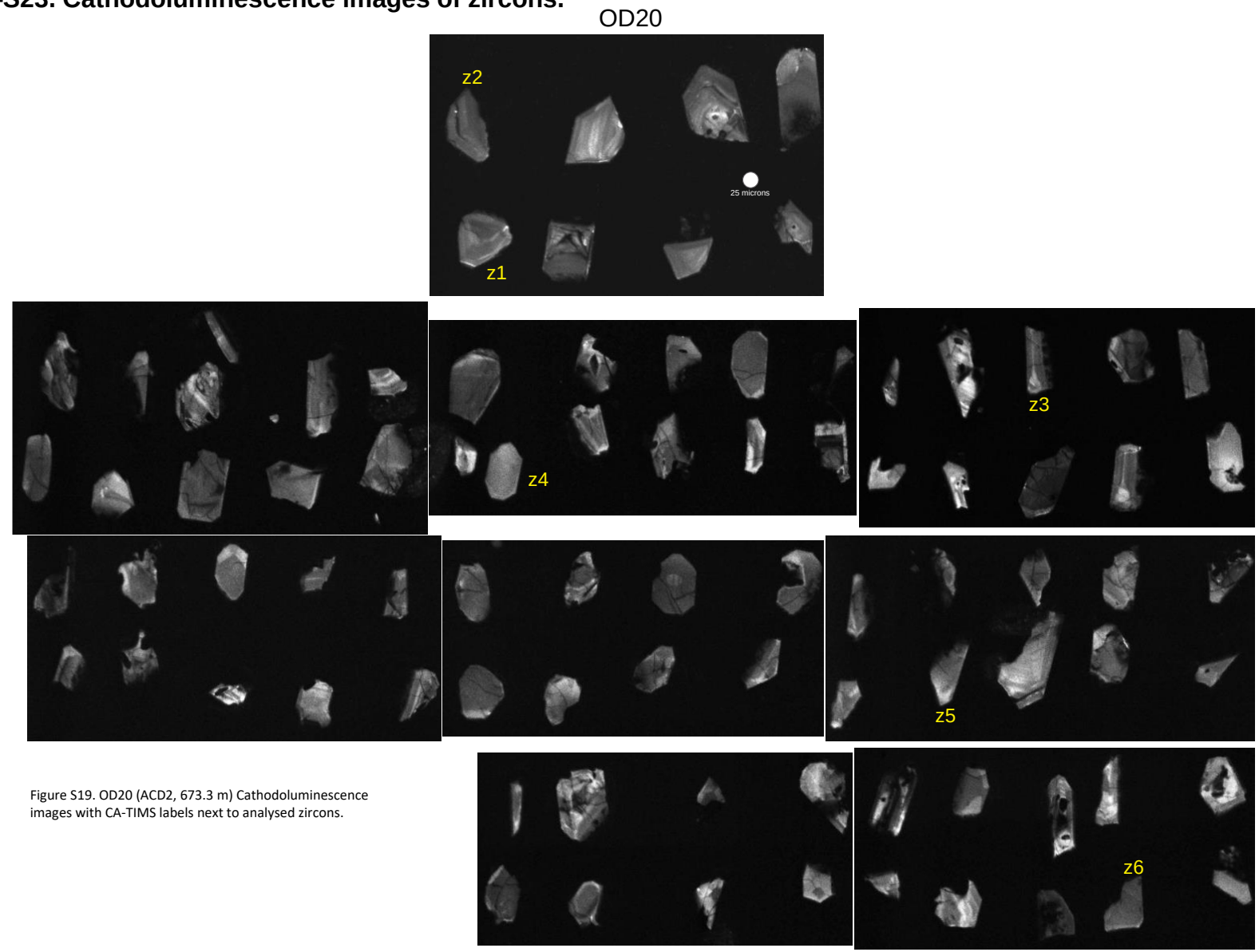

Figure S19. OD20 (ACD2, 673.3 m) Cathodoluminescence images with CA-TIMS labels next to analysed zircons.

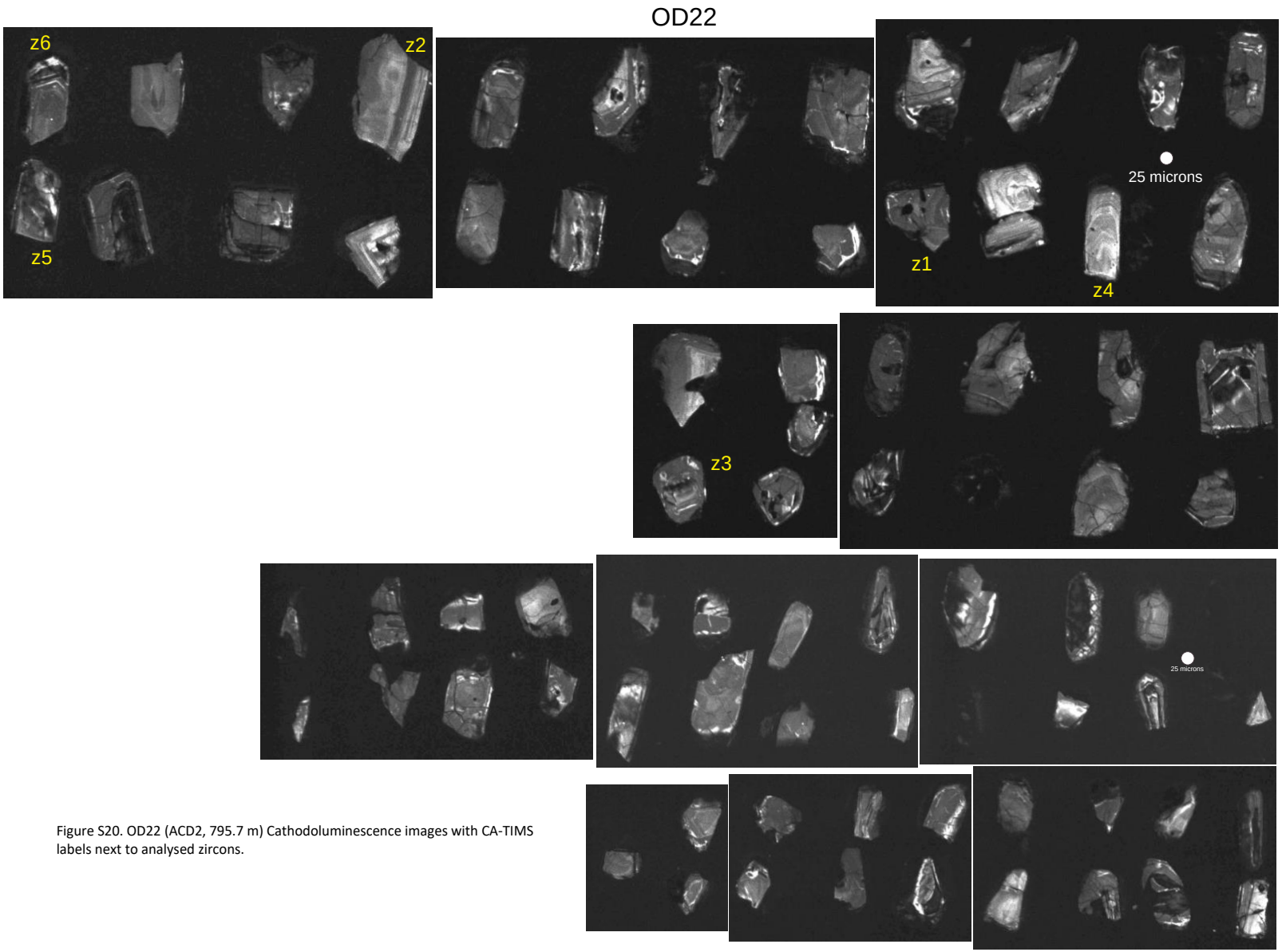

Figure S20. OD22 (ACD2, 795.7 m) Cathodoluminescence images with CA-TIMS labels next to analysed zircons.

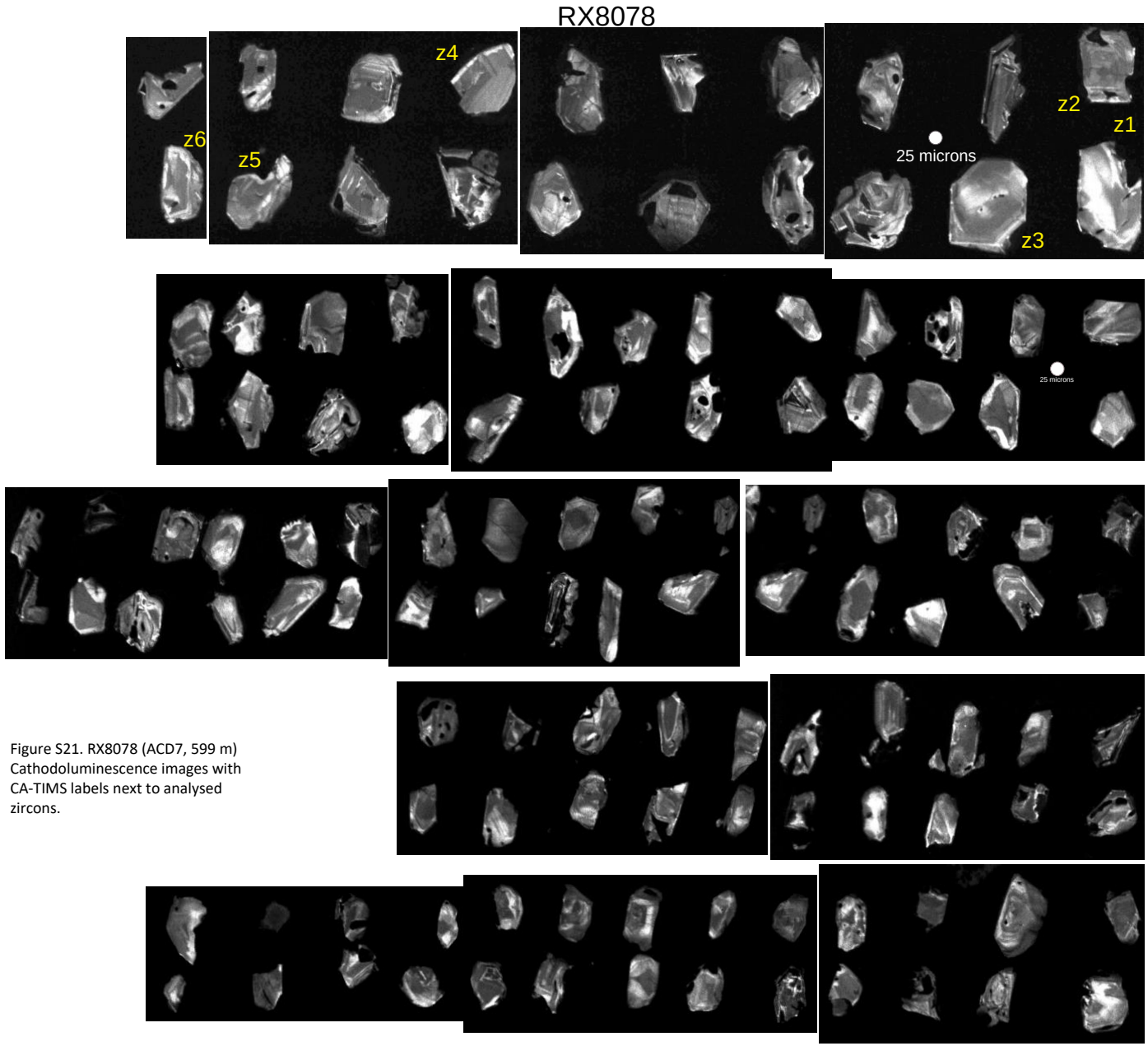

Figure S21. RX8078 (ACD7, 599 m) Cathodoluminescence images with CA-TIMS labels next to analysed zircons.

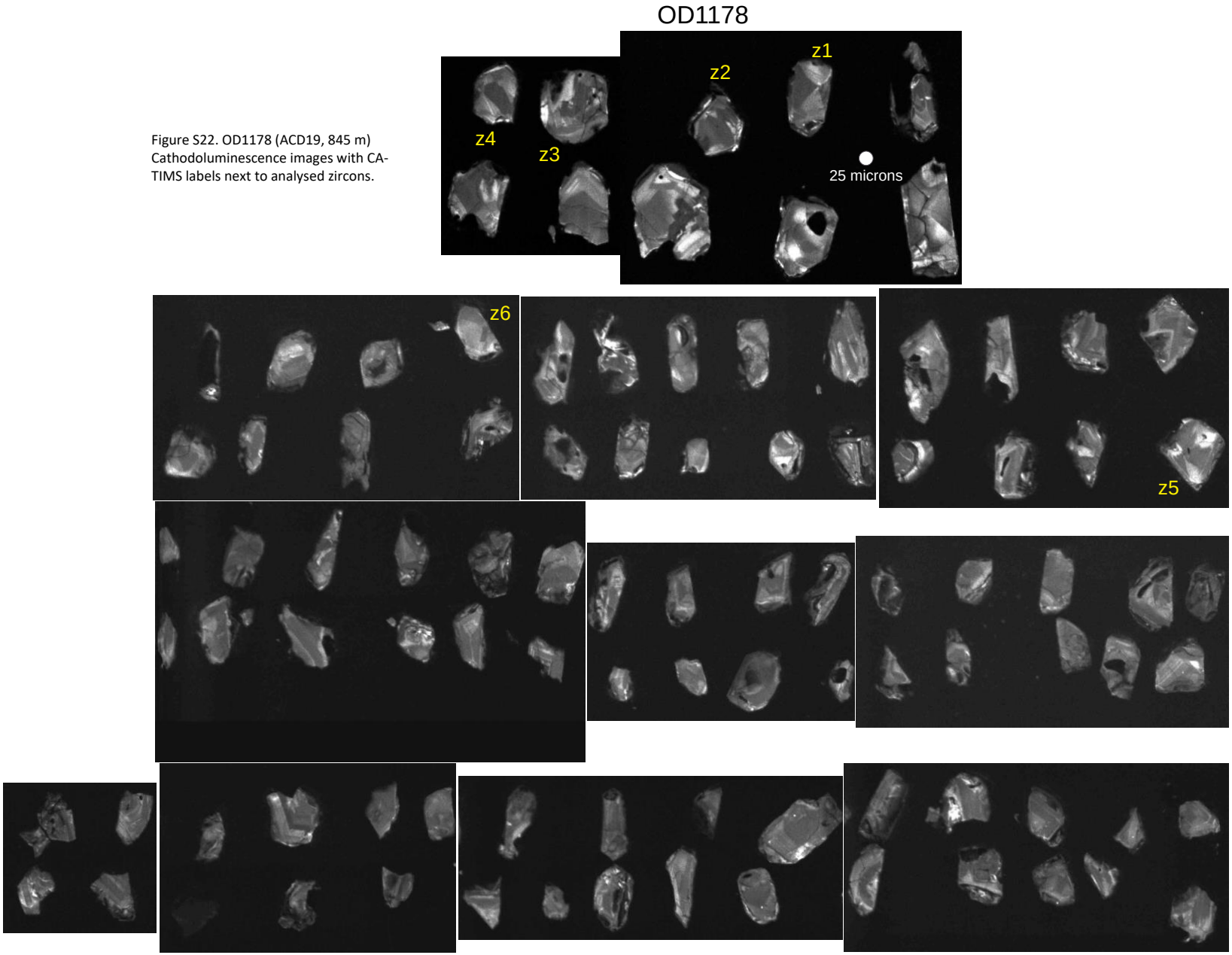

Figure S22. OD1178 (ACD19, 845 m) Cathodoluminescence images with CA-TIMS labels next to analysed zircons.

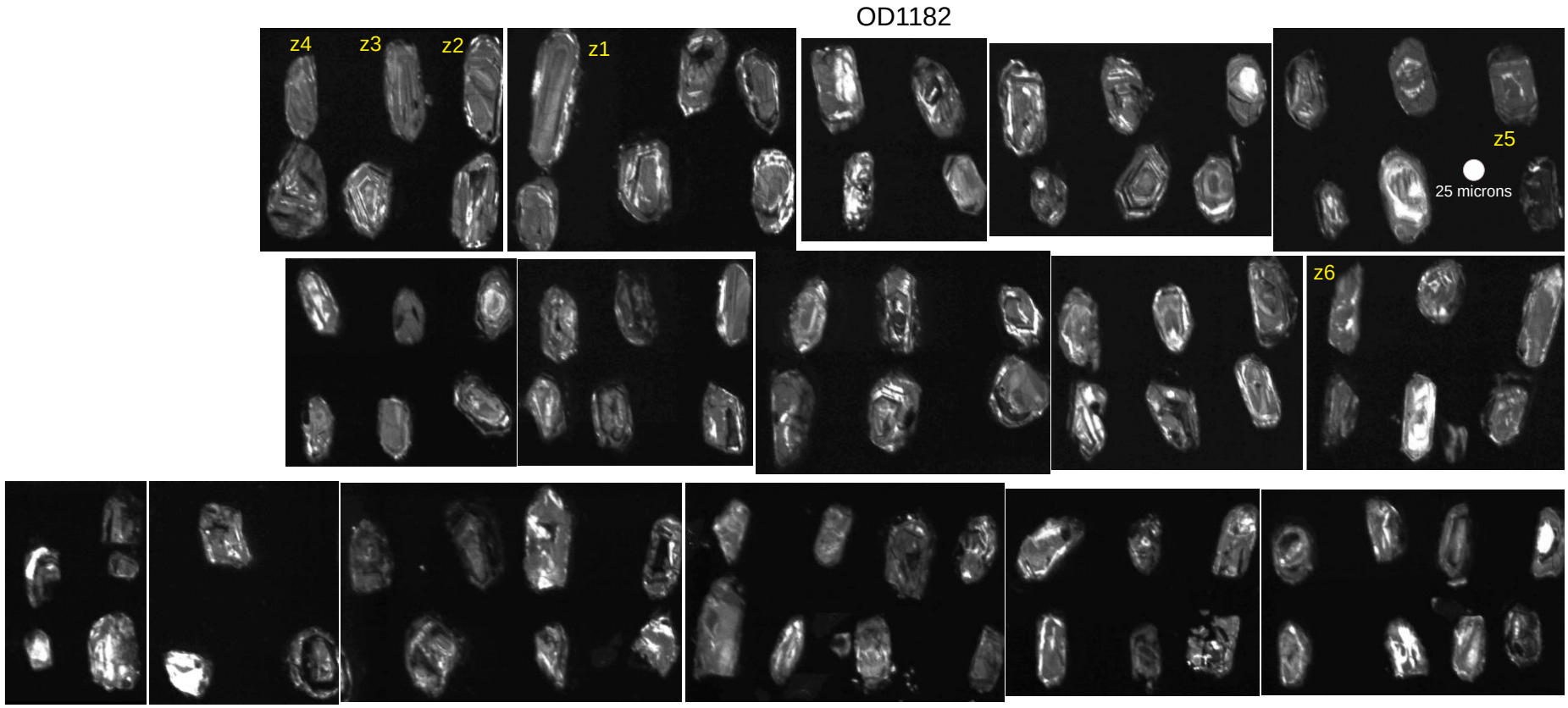

Figure S23. OD1182 (ACD19, 936.3 m) Cathodoluminescence images with CA-TIMS labels next to analysed zircons.

Figures S24–S26. Images of core samples

Figure S24. Pandurra Formation in ACD15, ~689 to 694 m. Interbedded fine to coarse quartz sandstone and red mudstone.

Figure S26. Donington Suite megacrystic granite in ACD3, 1011 to 1014 m.

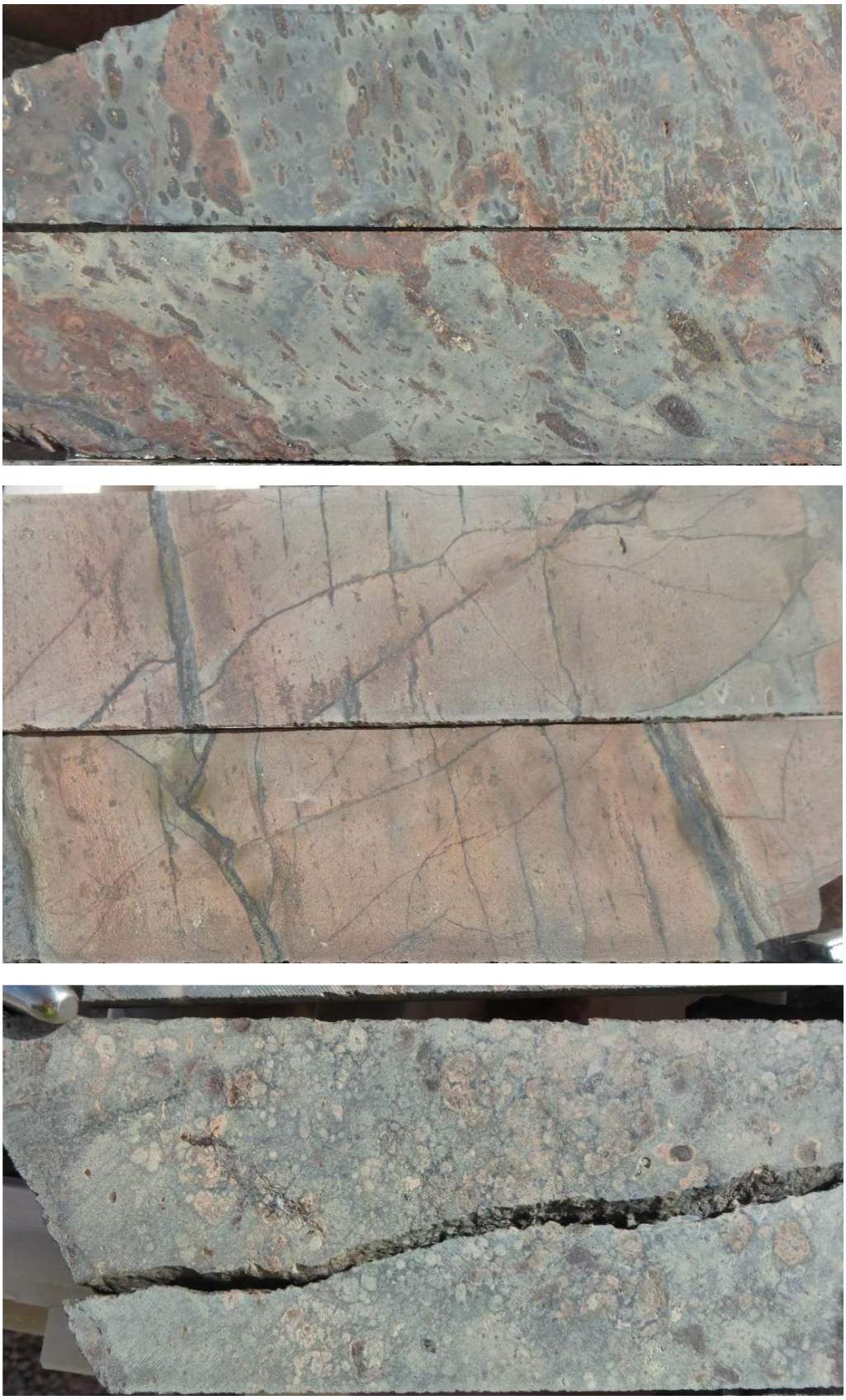

Figure S25. Groundmass textures in GRV felsic lavas. Top, altered amygdaloidal dacite, ACD20, 649 m; amygdales are elongate and aligned. Middle, flow-banded fine dacite, ACD20, 633 m. Lower, relic perlite (abundant round features are perlite cores) in altered fine dacite, ACD20, 529 m.

References

Amelin, Y., & Zaitsev, A. N. (2002). Precise geochronology of phoscorites and carbonatites. *Geochimica et Cosmochimica Acta, 66*, 2399–2419. doi:10.1016/S0016-7037(02)00831-1

Barfod, G. H., Krogstad, E. J., Frei, R., & Albarède, F. (2005). Lu–Hf and PbSL geochronology of apatites from Proterozoic terranes: A first look at Lu–Hf isotopic closure in metamorphic apatite. *Geochimica et Cosmochimica Acta, 69*, 1847–1859. doi:10.1016/j.gca.2004.09.014

Black, L. P., Kamo, S. L., Allen, C. M., Davis, D. W., Aleinikoff, J. N., Valley, J. W., . . .Foudoulis, C. (2004). Improved $^{206}Pb/^{238}U$ microprobe geochronology by the monitoring of a trace-element-related matrix effect; SHRIMP, ID-TIMS, ELA-ICP-MS and oxygen isotope documentation for a series of zircon standards. *Chemical Geology, 205*, 115–140. doi:10.1016/j.chemgeo.2004.01.003

Black, L. P., Kamo, S. L., Williams, I. S., Mundil, R., Davis, D. W., Korsch, R. J., & Foudoulis, C. (2003). The application of SHRIMP to Phanerozoic geochronology; a critical appraisal of four zircon standards. *Chemical Geology, 200*, 171–188. doi:10.1016/S0009-2541(03)00166-9

Cowley, W. M. (1993). Cariewerloo Basin. In J. F. Drexel, W. V. Preiss, & A. J. Parker (Eds). *The Geology of South Australia, Volume 1: The Precambrian* (pp. 139–142). Adelaide SA: Geological Survey of South Australia Bulletin 54.

Halpin, J. A., Jensen, T., McGoldrick, P., Meffre, S., Berry, R. F., Everard, J. L., . . . Whittaker, J. M. (2014). Authigenic monazite and detrital zircon dating from the Proterozoic Rocky Cape Group, Tasmania: Links to the Belt-Purcell Supergroup, North America. *Precambrian Research, 250*, 50–67. doi:10.1016/j.precamres.2014.05.025

Horstwood, M. S. A., Košler, J., Gehrels, G., Jackson, S. E., McLean, N. M., Paton, C., . . .Schoene, B. (2016). Community-derived standards for LA-ICP-MS U–(Th–)Pb geochronology – uncertainty propagation, age interpretation and data reporting. *Geostandards and Geoanalytical Research, 40*, 311–332. doi:10.1111/j.1751-908X.2016.00379.x

Huang, Q., Kamenetsky, V. S., McPhie, J., Ehrig, K., Meffre, S., Maas, R., . . . Hu, Y. (2015). Neoproterozoic (ca. 820–830 Ma) mafic dykes at Olympic Dam, South Australia: Links with the Gairdner Large Igneous Province. *Precambrian Research, 271*, 160–172. doi:10.1016/j.precamres.2015.10.001

Jagodzinski, E. A. (2005). *Compilation of SHRIMP U–Pb geochronological data, Olympic Domain, Gawler Craton, South Australia, 2001–2003*. Canberra ACT: Geoscience Australia, Record 2005/20, 197 p.

Ludwig, K. R. (2008). *User's manual for Isoplot 3.70: A geochronological toolkit for Microsoft Excel.* Berkeley Geochronological Center Special Publication. Berkeley, CA: University of California.

McDowell, F. C., McIntosh, W. A., & Farley, K. (2005). A precise $^{40}Ar–^{39}Ar$ reference age for the Durango apatite (U–Th)/He and fission-track dating standard. *Chemical Geology, 214*, 249–263. doi:10.1016/j.chemgeo.2004.10.002

Paton, C., Woodhead, J. D., Hellstrom, J. C., Hergt, J. M., Greig, A., & Maas, R. (2010). Improved laser ablation U–Pb zircon geochronology through robust downhole fractionation correction. *Geochemistry, Geophysics, Geosystems, 11*(3). https://doi.org/10.1029/2009GC002618

Schoene, B. A., & Bowring, S. A. (2006). U–Pb systematics of the McClure Mountain syenite: Thermochronological constraints on the age of the $^{40}Ar/^{39}Ar$ standard MMhb. *Contributions to Mineralogy and Petrology, 151*, 615–630.doi:10.1007/s00410-006-0077-4

Sláma, J., Kosler, J., Condon, D. J., Crowley, J. L., Gerdes, A., Hanchar, J. M., . . . Whitehouse, M. J. (2008). Plešovice zircon — A new natural reference material for U–Pb and Hf isotopic microanalysis. *Chemical Geology, 249*, 1–35. doi:10.1016/j.chemgeo.2007.11.005

Thompson, J., Meffre, S., Maas, R., Kamenetsky, V. S., Kamenetsky, M. B., Goemann, K., . . . Danyushevsky, L. (2016). Matrix effects in Pb/U measurements during LA-ICP-MS analysis of the mineral apatite. *Journal of Analytical Atomic Spectrometry, 31*, 1206–1215. doi:10.1039/C6JA00048G

Thompson, J. M., Meffre, S., & Danyushevsky, L. (2018). Impact of air, laser pulse width and fluence on U–Pb dating of zircons by LA-ICPMS. *Journal of Analytical Atomic Spectrometry, 33*, 221–230. doi:10.1039/C7JA00357A

Wiedenbeck, M., Alle, P., Corfu, F., Griffin, W. L., Meier, M., Oberli, F., . . . Spiegel, W. (1995). Three natural zircon standards for U–Th–Pb, Lu–Hf, trace element and REE analyses. *Geostandards Newsletter, 19*, 1–23. https://doi.org/10.1111/j.1751-908X.1995.tb00147.x